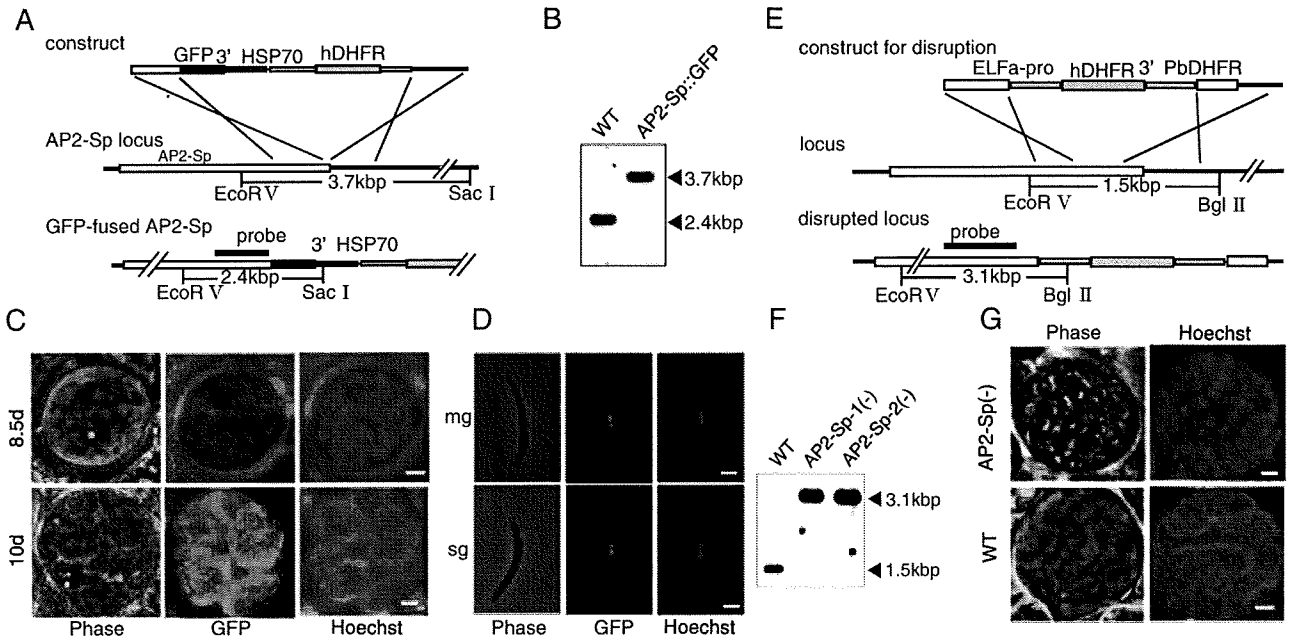

Fig. 1. AP2-Sp is necessary for sporozoite formation.
A. Preparation of parasites expressing AP2-Sp tagged with GFP. The targeting construct (upper) was inserted into the 3′-end of the endogenous AP2-Sp gene locus (middle) by homologous recombination. Transformed parasites (lower) were selected by pyrimethamine-resistance.
B. Southern blot analysis of AP2-Sp::GFP parasites. WT and AP2-Sp::GFP genomic DNA was digested with EcoRV and SacI and hybridized with the probe indicated by a solid bar in (A). WT, original wild-type parasites.
C. Upper panels: Oocyst of AP2-Sp::GFP parasites 8.5 days after an infective blood meal. Fluorescent signals of GFP were colocalized with spotted nuclei stained with Hoechst. Phase, phase-contrast image. Lower panels: Oocyst 10 days after infective blood meal. Scale bars, 5 μm.
D. Oocyst and salivary gland sporozoites of AP2-Sp::GFP parasites. GFP signals are localized in the nuclei of both stages. Scale bars, 2 μm.
E. Targeted disruption of the AP2-Sp gene. Targeting construct (upper) was inserted into the AP2-Sp gene locus (middle) by homologous recombination.
F. Southern blot analysis was carried out on AP2-Sp (–) parasite populations (1 and 2) that were independently prepared. WT and AP2-Sp (–) genomic DNA was digested with EcoRV and BglII and hybridized with the probe indicated by a solid bar in (E).
G. Oocysts of wild-type (WT) and AP2-Sp (–) 1 parasites 10 days after an infective blood meal. Midguts infected with wild-type or knockout parasites were stained with Hoechst. Budding sporozoites were not observed around sporoblasts in AP2-Sp (–) oocysts (upper panels), while numerous sporozoites budding from sporoblasts were stained with Hoechst in WT oocysts (lower panels). Scale bars, 5 μm.

proliferation in the blood stage but is essential for formation of sporozoites.

Results

AP2-Sp is expressed from the late oocyst to the salivary gland sporozoite

To search for AP2-related genes expressed in sporozoites, we screened our *P. berghei* EST (expressed sequence tag) database [available at the PlasmoDB website (http://www.plasmodb.org)] and found that ESTs of *AP2-Sp* (PlasmoDB identifier, PB000752.01.0) are present in oocyst and salivary gland sporozoites (1 and 3 ESTs, respectively). We therefore prepared transgenic parasites that expressed GFP-tagged AP2-Sp in *P. berghei* (AP2-Sp::GFP parasites, Fig. 1A and B) and investigate the expression profile of *AP2-Sp*. In AP2-Sp::GFP parasites, GFP signals were not observed in the blood stages, including gametocytes and ookinetes cultured *in vitro* (Fig. S1). In the mosquito vector, however, fluorescent signals appeared in some oocysts 6 days after an infective blood meal (or fertilization), and the proportion of oocysts expressing AP2-Sp::GFP increased with time (Table S1). In these oocysts signals were weak and localized in Hoechst-stained spotted nuclei of sporoblasts (Fig. 1C, upper panels). Around 10 days after an infective blood meal, new, strong GFP signals appeared in oocysts (Fig. 1C, lower panels). These signals were localized to the nuclei of sporozoites budding from sporoblasts and therefore displayed ring-like appearances around the core of the sporoblasts. Strong GFP signals were further observed in the nucleus of sporozoites released from oocysts (oocyst sporozoites) and in sporozoites harvested from mosquito salivary glands (salivary gland sporozoites) (Fig. 1D). These results suggested that this protein would function as a TF in the sporozoite stage.

Table 1. Formation of oocysts and sporozoites in AP2-Sp (–) parasites.

Parasite populations	Number of oocysts per mosquito (mean ± SE, $n = 20$)	Diameter (μm) of oocysts (mean ± SE, $n = 50$)	Number of oocyst sporozoites per mosquito	Number of salivary gland sporozoites per mosquito
Wild type	112.95 ± 36.17	133.75 ± 3.76	26235 ± 2095[a]	10750 ± 472[a]
AP2-Sp (–) 1	115.05 ± 43.00	130.91 ± 3.28	1.8, 0.9[b]	0, 0[b]
AP2-Sp (–) 2	107.65 ± 30.21	138.06 ± 2.59	3.6, 0.9[b]	0, 0[b]

a. Twenty mosquitoes were dissected, and sporozoites were counted using a haemocytometer. Each value is a mean of three independent experiments ± SE.
b. Fifty mosquitoes were dissected, and sporozoites were counted using a haemocytometer. Two independent experiments were performed in each population.

AP2-Sp is necessary for the formation of sporozoites in oocysts

Next, we performed targeted disruption of *AP2-Sp* in *P. berghei* (Fig. 1E and F). Two knockout populations were obtained from independent transfection experiments. The knockout populations replicated normally in the blood, developed into ookinetes and infected the mosquito midgut; the number and sizes of oocysts formed in the midgut were essentially the same as in the wild type (Table 1). In the oocysts, however, sporozoites were not observed, even 14 days after the infective blood meal and were barely detectable after harvest from the midgut (Table 1). Nuclear staining with Hoechst showed that the nucleus of each oocyst was divided into several small nuclei 10 days after the infective blood meal in knockout as in wild-type parasites (Fig. 1G). Semithin sections stained with Giemsa, however, revealed that the subsequent invagination of the plasma membrane, which is necessary for formation of sporoblasts, did not occur in knockout parasites even 14 days after infective blood meal (Fig. S2). These results suggested that AP2-SP is involved in the expression of genes necessary for sporozoite formation.

AP2-Sp binds to eight bp sequences containing TGCATG

In our previous paper (Yuda *et al.*, 2009), we reported that AP2-O binding sites in a promoter have the following two features; they are located immediately upstream of the transcription start site (TSS), and usually two or more binding sites are present. According to these observations, we explored putative *cis*-acting elements in sporozoite-specific genes. We found that the six-base sequence, TGCATG, and its reverse complimentary sequence, CATGCA, were frequently found in the upstream regions of these sporozoite-specific genes. In particular, a conjugated palindromic sequence, TGCATGCA, was found at high frequencies in them (see also Fig. 3A). The sequence is identical to the sequence that was recently reported to be a common upstream motif of sporozoite genes in *P. falciparum* (Young *et al.*, 2008). The conjugated eight-base sequence is identical to the sequence that has been reported as a binding sequence for the AP2 domain of *P. falciparum* AP2-Sp (PF14_0633) (De Silva *et al.*, 2008).

We next examined whether the AP2 domain of *P. berghei* AP2-Sp binds to the six-base sequence using EMSA (electrophoretic mobility-shift assay). Because the AP2 domain of AP2-Sp has an adjacent AT-hook motif (Balaji *et al.*, 2005) and this region might participate in binding, recombinant AP2 domains with and without the AT-hook region were tested. As a probe, a 192 bp region upstream of the *MAEBL* gene, a sporozoite-specific gene essential for salivary gland infection (Kariu *et al.*, 2002), was used. This region contained a single TGCATGCA site. As shown in Fig. 2A, EMSA generated clearly shifted bands for both recombinant proteins. However, addition of a single mutation to the putative binding sequence (TGCATGCA to TGGATGCA) virtually abolished these bands. This result indicated that the AP2 domain specifically recognizes this sequence.

Next, we designed short (29 bp) double-stranded oligonucleotide probes from the region around the TGCATG site upstream of *MAEBL*. These probes contained various point mutations, to determine the sequence necessary for binding to the AP2 domain (Fig. 2B). Only GST-fused proteins, without the AT-hook region, were used in these assays, because there seemed to be no difference in binding properties between the two recombinant proteins. The results indicated that CATG is a core sequence essential for binding (Fig. 2B, left and centre panels) and that the two bases either side of this sequence also participate in binding (Fig. 2B, left panel), i.e. the whole palindromic sequence of eight bases, TGCATGCA, is involved in the binding of the AP2 domain. The minimum sequence essential for binding the AP2 domain was TGCATG, because, binding was abolished only when both TGCATG and its reverse complementary sequence CATGCA were mutated at the same time (Fig. 2B, centre panel). A mutation to either side of the sequence had no affect on binding (Fig. 2B, right panel).

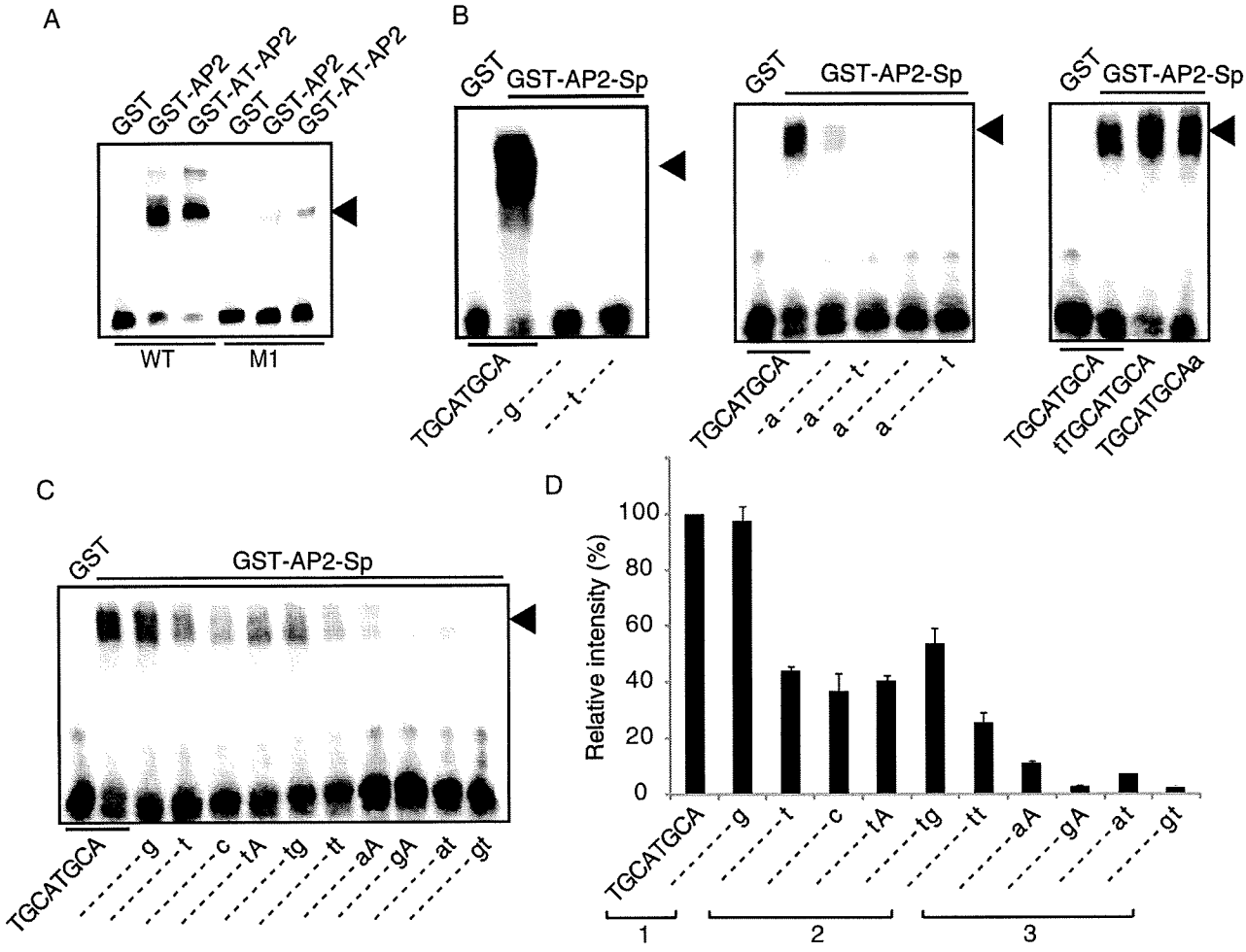

Fig. 2. AP2 domain of AP2-Sp recognizes eight-base sequences beginning with TGCATG.
A. EMSA was performed with the GST-fused AP2 domain of AP2-Sp, with and without the AT-hook region (GST-AT-AP2 and GST-AP2 respectively). The upstream region of *MAEBL* (192 bp), which contains one TGCATGCA sequence, was used as a probe (WT). A point mutation (TGCATGCA to TGGATGCA) in this probe (M1) nearly abolished the shifted band (arrow head). GST was used as a control.
B. EMSA was performed with the GST-fused AP2 domain of AP2-Sp without the AT-hook region. Oligonucleotide probes (29 bp) were designed based on the upstream region of *MAEBL* around the TGCATGCA sequence. Mutations added to this probe are indicated under each lane with small characters. A mutation to CATG at the center of TGCATGCA abolished the shifted band (left panel). A mutation to either TG or CA at the end of TGCATGCA significantly reduced the shifted band, and mutations to both ends together abolished the shifted band (centre panel). Mutation of the bases beside TGCATGCA had no affect on binding (right panel).
C and D. Three independent EMSAs were performed with oligonucleotide probes that are different from the original probe in (B) at either or both of the two bases following TGCATG. One of the electrophoresis images obtained in these assays is shown in (C). Intensities of shifted bands were measured with a densitometer, and the averages of three assays are shown in a bar graph with standard errors in (D). The sequences of oligonucleotide probes were roughly divided into three groups according to the band intensities, as indicated under the graph.

These results suggest that AP2-Sp could bind to several eight-base sequences beginning with TGCATG but that binding properties would vary among them. We therefore compared binding affinities among these sequences using 29 bp short oligonucleotide probes (Fig. 2C and D). The results showed that binding sequences for the AP2 domain could be roughly divided into three groups according to binding properties. The first group is composed of TGCATGCA and TGCATGCG, to which the AP2 domain binds most tightly. The second group contains four sequences, TGCATGCC/T and TGCATGTA/G, which are identical to the sequences of the first group at seven bases and have lower affinities. The third group includes other sequences containing TGCATG that also resulted in a shifted EMSA band, although with lower binding affinities than the former two groups.

Figure 3A illustrates these binding sequences in 1 kb upstream regions (and 1.2 kb regions in some genes) of sporozoite-specific genes and the most upstream ESTs, which indicate the putative TSS of each gene. All of these genes have one of the eight-base sequences in the upstream region (over half of them have the eight-base sequences belonging to the first group), and transcription

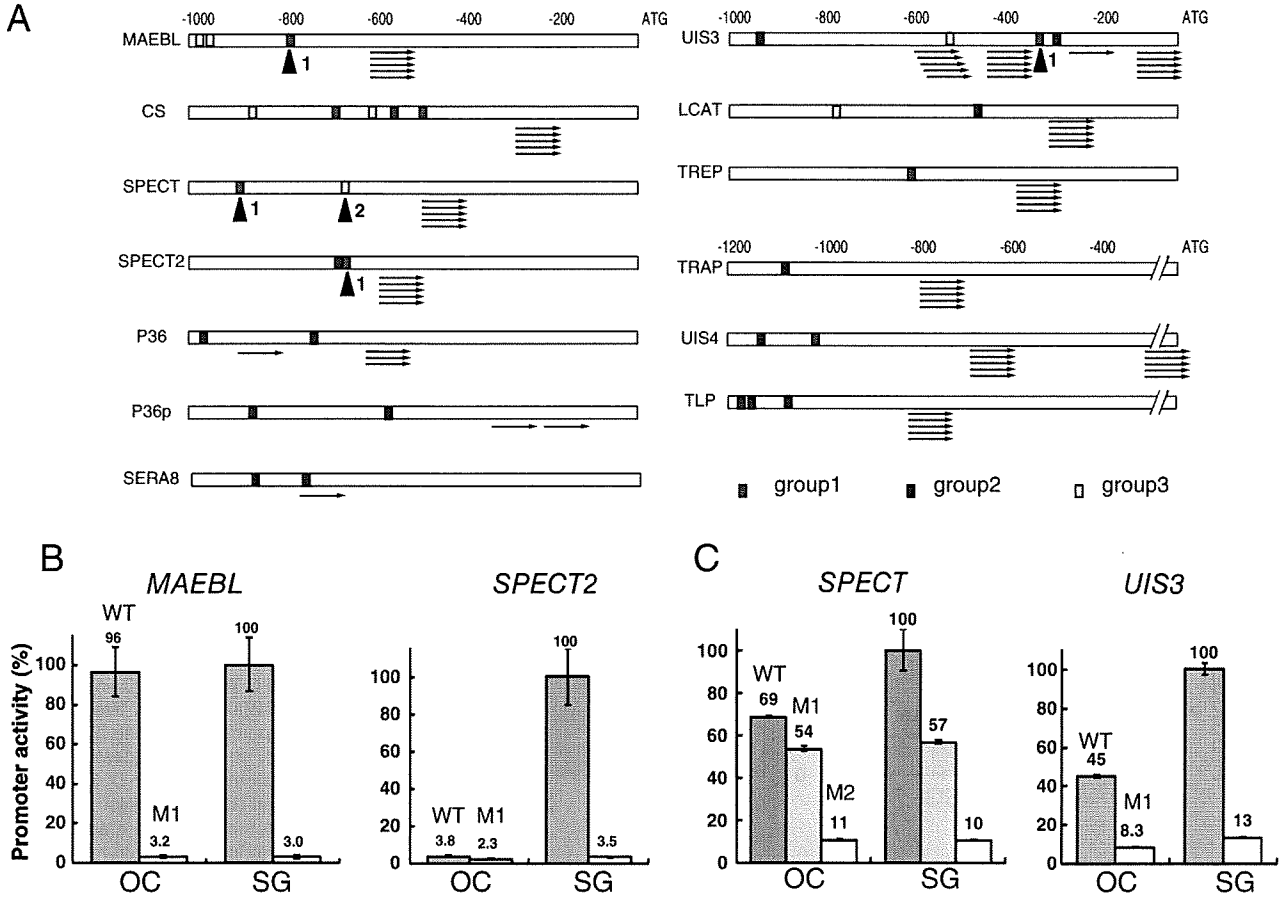

Fig. 3. Promoter activities of sporozoite-specific genes are dependent on AP2-Sp binding to sequences in the upstream region.
A. Binding sequences for AP2-Sp (rectangles) and start sites of most upstream ESTs (arrows), which indicate TSS, in the 1 kb region upstream of sporozoite-specific genes. Binding sequences are coloured according to the groups to which they belong (see also Fig. 2D). In some genes with a long 5′-untranslated region (lower right), 1.2 kb upstream regions are shown. In most genes transcription starts 100–300 bp downstream of a binding site for AP2-Sp, and two or more binding sites are usually within the 1 kb region upstream of the first ATG codon. EST data are available at the PlasmoDB website. Arrowheads indicate binding sequences that were mutated in reporter assays in (B) and (C).
B. Reporter assays of *MAEBL* and *SPECT2* were performed *in vivo* with pCen-GFP. Promoter activities in oocyst (OC) and salivary gland (SG) sporozoites were compared between original (WT) and mutated (M1) promoters. In both genes, a point mutation was added to the binding sequence for AP2-Sp (TGCATGCA to TGGATGCA) in the upstream region.
C. The reporter assays of *SPECT* and *UIS3* were performed using pCen-Luc. A mutation was added to one [numbered 1 in (A), M1] or two binding sites (1 and 2, M2) in *SPECT* and to one binding site (M1) in *UIS3*. Results were expressed as a percentage of the original activity in salivary gland sporozoites.

of these genes starts 100–300 bp downstream of the binding sequences. Computational analyses in 1 kb upstream regions of 13 genes, which have been reported sporozoite-specific, demonstrated that the six-base sequence occurs at high frequencies in these genes (Table S2). These results strongly suggest that binding sequences for AP2-Sp act as common *cis*-acting elements in the upstream regions of sporozoite-specific genes and that they are usually located in the proximal promoter region of these genes. These features are similar to those of AP2-O, which we reported previously (Yuda *et al.*, 2009). We also found that some eight-base sequences beginning with CGCATG can be binding sequences for AP2-Sp (data not shown). However, we omitted these sequences from the following analyses because the frequencies of these GC-rich sequences in the genome are very low (an example that such sequences act as *cis*-acting motifs *in vivo* is shown in the promoter analysis of PB000863.01.0 in Fig. 4B).

TGCATGCA is a cis*-acting element specific for the sporozoite stage*

We next examined whether the eight-base sequences act as *cis*-acting elements in the sporozoite stage using *in vivo* promoter assays (Fig. 3B and C). First, we tested TGCATGCA in the upstream region of *MAEBL* (Fig. 3B). For this assay we used the *P. berghei* centromere plasmid

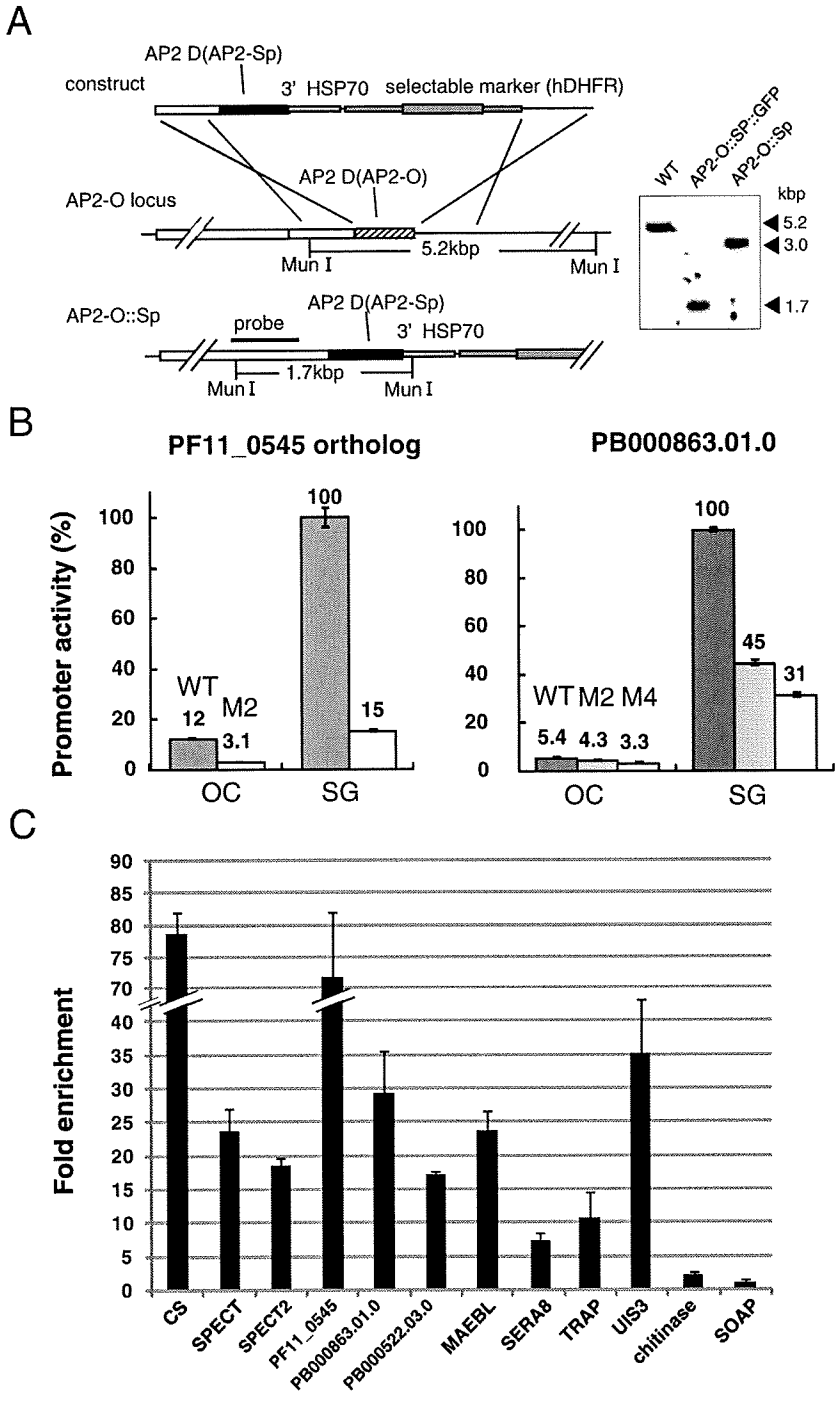

Fig. 4. Induction of AP2-Sp target genes in ookinetes.
A. Preparation of AP2-O::Sp parasites. DNA construct containing the coding region of the AP2 domain of AP2-Sp (upper) was inserted in frame into the 3′-end of the endogenous AP2-O gene (middle) by homologous recombination, resulting in the swap of the region encoding the AP2 domain of AP2-O with the region encoding the AP2 domain of AP2-Sp (lower). Preparation of AP2-O::Sp::GFP parasites was carried out with the same procedure but using a construct containing the coding region of the AP2 domain of AP2-Sp followed by the GFP gene. Results of Southern hybridization with the probe indicated by a solid bar are shown in the right panel.
B. Reporter assays were performed with the artificial chromosome pCen-Luc. Promoter activities in oocyst (OC) and salivary gland (SG) sporozoites were compared between the original upstream region (WT) and regions containing point mutations at binding sites for AP2-Sp. The binding sites mutated were TGCATGCG and TGCATGCT (M2, see also Fig. 3S) in PF11_0545 orthologue, and two TGCATGTGs (1 and 2 in Fig. 3S, M2) and CGCATGTT and CGCATGTG (3 and 4 in Fig. 3S, M4) in PB000863.01.0. Results were expressed as a percentage of the original activity in salivary gland sporozoites.
C. ChIP was performed in AP2-O::Sp::GFP parasites with anti-GFP antibodies. Precipitated DNA fragments were analysed by qPCR using primers for upstream regions of 11 genes including those induced in AP2-O::Sp parasites (*SPECT*, *SPECT2*, PF11_0545 orthologue, PB000522.03.0 and PB000863.01.0), other known sporozoite-specific genes (*TRAP*, *MAEBL*, *UIS3* and *SERA8*) and ookinete-specific genes (*chitinase* and *SOAP*) as controls. Percentage of input of each gene is shown in Table S8.

pCen-GFP, which contains the GFP reporter gene (Fig. S3A) (Yuda *et al.*, 2009). Reporter constructs made in this plasmid are retained through the sporozoite stage by approximately 90% of parasites without drug selection, having been introduced into asexual blood stages by electroporation (S. Iwanaga *et al.*, unpubl. results). In parasites transfected with pCen-GFP containing the *MAEBL* promoter, strong GFP signals were observed in oocyst sporozoites. The signal intensity reached a peak in this stage, which was in accordance with the expression profile of the *MAEBL* gene *in vivo*. Addition of a point mutation to the eight-base sequence (TGCATGCA to TGGATGCA) decreased the signals intensity to the background level, indicating that this sequence is critical for promoter activity. Next, we tested the upstream region of *SPECT2*, which also contains a single TGCATGCA site

(Fig. 3B, right). *SPECT2* is necessary for skin and liver invasion and is predominantly expressed in the salivary gland sporozoite (Ishino *et al.*, 2005; Amino *et al.*, 2008). In parasites transfected with pCen-GFP containing the *SPECT2* promoter, GFP signals were weak in oocyst sporozoites but increased approximately 20 times after salivary gland infection. This steep increase in promoter activity coincides well with the expression profile of *SPECT2*. Addition of a point mutation to the motif decreased GFP signals to background levels in both oocyst sporozoites and salivary gland sporozoites.

The promoter region of sporozoite-specific genes usually has multiple binding sites for AP2-Sp. To examine how these individual sequences contribute to the overall promoter activity, we next performed promoter assay with pCen-Luc in the *SPECT* promoter (Fig. 3C, left) (Ishino *et al.*, 2004) where two putative *cis*-acting elements different from TGCATGCA tested above (TGCATGCG and TGCATGTT) are present (Fig. 3A). In these assays luciferase was used as a reporter (pCen-Luc, Fig. S3B) instead of GFP to assess promoter activity more quantitatively. The activity of the *SPECT* promoter decreased according to the number of binding sites that were mutated. This indicated that both TGCATGCG and TGCATGTT act as *cis*-acting elements and that these elements additively affect promoter activity. The additive effect on promoter activity was similar to that reported for AP2-O binding sequences in the ookinete stage (Yuda *et al.*, 2009).

We also tested the promoter of *UIS3* (upregulated in infective sporozoites gene 3) (Mueller *et al.*, 2005) (Fig. 3C, right). *UIS3* is upregulated in salivary gland sporozoites and is also expressed in the liver stage. Therefore, the expression profile and function is different from the three genes tested above. Addition of a mutation to the single TGCATGCA site significantly decreased promoter activity of the *UIS3* upstream region in both oocyst and salivary gland sporozoites. These results together with those described above demonstrated that the eight-base sequence acts as a critical *cis*-acting element, irrespective of whether the peak activities of the promoter are present in oocyst or salivary gland sporozoites.

Induction of AP2-Sp target genes in the ookinete stage

The results presented above indicated that AP2-Sp is a *trans*-acting factor that induces sporozoite-specific genes. However, it was unknown whether this protein directly binds to the promoter of these genes *in vivo*. ChIP-qPCR (chromatin immunoprecipitation with quantitative PCR) analysis is an appropriate technique to demonstrate this. However, we were unable to obtain sufficient parasites for this analysis. Indeed, we attempted a ChIP assay with sporozoites that were harvested from 300 infected mosquitoes (approximately 6×10^6 sporozoites), but insufficient chromatin DNA for subsequent qPCR analysis was recovered (data not shown).

To conquer this problem, we prepared parasites that expressed endogenous *AP2-O*, but whose AP2 domain had been swapped with that of AP2-Sp (AP2-O::Sp parasites and AP2-O::Sp::GFP parasites, Fig. 4A), and examined (i) whether the chimeric TF might induce target genes of AP2-Sp in the ookinete stage and (ii) whether the TF would bind to the promoter regions of sporozoite-specific genes. To assess the induction, we analysed gene expression by microarray analysis of ookinetes using AP2-O::Sp parasites and selected genes whose expression increased over threefold compared with *AP2-O* (–) parasites. The microarray analysis showed that expression increased in 33 genes (Table S3). They were composed of six sporozoite-specific genes [*SPECT*, *SPECT2*, *CS*, *TLP* (TRAP-like protein), S10 and S23], whose expression in sporozoites has been demonstrated or suggested (Matuschewski *et al.*, 2002; Ishino *et al.*, 2004; 2005; Moreira *et al.*, 2008), and 27 novel genes whose expression has not been reported in the sporozoite stage. Computational analysis of upstream regions of the 30 genes (upstream regions of three genes were not obtained from the *P. berghei* genome database) showed that sequences containing TGCATGCA occurred at significantly high frequencies, indicating that direct binding of the TF to these regions could induce these genes (Table S4). Figure S3 illustrates the binding sites for AP2-Sp in the upstream regions of the 26 genes that are not in Fig. 3A. Of the 30 genes, 19 had at least one binding site belonging to the first group (TGCATGCA, TGCATGCG and their reverse complementary sequences, see also Table S3), and 17 genes had at least one binding site belonging to the second group (TGCATGTG, TGCATGTA, TGCATGCT, TGCATGCC and their reverse complementary sequences). The most upstream ESTs of each gene (Fig. S3) indicated that transcription of these genes starts approximately 100–300 bp downstream of the binding sequences, as was observed for the sporozoite-specific genes in Fig. 3A.

We performed further promoter assays to confirm that these genes really are under the control of AP2-Sp in the sporozoite stage (Fig. 4B). We tested two genes. One of the genes we tested currently has no gene ID in PlasmoDB (in *P. falciparum* PlasmoDB identifier, PF11_0545, has been attributed to the orthologue). The upstream region of this gene had a single binding sequence, TGCATGCG, and ESTs of this gene were mainly present in salivary gland sporozoites (Fig. S4 and Table S3). The promoter activity of this gene increased after salivary gland infection, and addition of a mutation (TGCATGCG to TGGATGCG) significantly decreased the activity in both oocyst and salivary gland sporozoites. Another gene

we tested (PlasmoDB identifier: PB000863.01.0) was a member of the AP2-related gene family and has an orthologue in *P. falciparum* (PlasmoDB identifier: PFD0985w). This gene has four putative *cis*-acting elements in the upstream region, two TGCATGTG and two CGCATGTG (Fig. S4), and ESTs of this gene were present mainly in salivary gland sporozoites (Table S3). Promoter activity of this gene increased steeply after salivary gland infection, and point mutations to the motifs (in two and four motifs) reduced the activity stepwise. These results indicated that expression of these two genes is controlled by AP2-Sp in the sporozoite stage.

We then examined direct binding of the chimeric TF to the promoter region of these genes by ChIP-qPCR assays using parasites expressing the chimeric TF fused with GFP at the C-terminus (AP2-O::SP::GFP parasites). In these parasites, GFP signals were detected in the nucleus of ookinetes, as was seen in AP2-O::GFP parasites (data not shown). As shown in Fig. 4C, IP with antibodies against GFP significantly enriched the upstream regions of sporozoite-specific genes, including those induced in AP2-O::SP parasites (*SPECT*, *SPECT2*, *CS*, *P. berghei* orthologue of PF11_0545, PB000863.01.0 and PB000522.03.0) and also *MAEBL*, *UIS3*, *TRAP* and *SERA* (serine repeat antigen) *8*/egress cysteine protease 1 (Aly and Matuschewski, 2005), which were not significantly induced in AP2-O::SP parasites. In contrast, binding to the upstream regions of *SOAP* (secreted ookinete adhesive protein) and *chitinase*, which are ookinete-specific genes (Dessens *et al.*, 2003), were not observed. These results demonstrated that the AP2 domain of AP2-Sp specifically binds to the upstream region of sporozoite-specific genes *in vivo*.

Discussion

Proteins expressed in sporozoites are potential targets for vaccine development, but the mechanisms of gene regulation in this stage remain poorly understood. Here we have provided evidence that the AP2 family TF, AP2-Sp, widely regulates gene expression in the sporozoite stage. This TF is expressed in the period from the late oocyst to the salivary gland sporozoite and induces the expression of genes with various functions and expression profiles. Target genes of this TF include all known genes specifically expressed in sporozoites, suggesting that this TF plays a central role in gene regulation of the sporozoite stage. We also demonstrated that AP2-Sp induces these target genes by binding to specific *cis*-acting elements in proximal promoter regions and that these elements are critical for promoter activity of each gene.

In a previous paper we reported that another AP2 family TF, AP2-O, regulates gene expression in the ookinete stage. Similar to AP2-Sp, Ap2-O directly activates several genes, including all known genes specifically expressed in the ookinete stage. AP2-O also shares some unique features of gene activation with AP2-Sp, such as binding to the proximal promoter region and additive effects of binding sites with respect to promoter activity. This indicates that mechanisms of gene regulation are closely related in these two stages.

However, a difference in gene expression between these two stages is that the sporozoite stage is composed of two forms with distinct infection ability, salivary and oocyst sporozoites, and thus target genes of AP2-Sp include those exhibiting distinct expression patterns such as *MAEBL* and *SPECT2*. Because such distinct expression patterns are difficult to explain solely by interactions between AP2-Sp and its binding sites on the promoter, there may be other TFs or co-regulators that modulate the function of AP2-Sp. Whereas at present we have not yet succeeded in identifying them, further investigation of AP2 family TFs in this stage and promoter analysis of genes exhibiting distinct expression patterns using the centromere plasmid might answer the question of how *Plasmodium* sporozoites change infection capability in the mosquito.

AP2-Sp (–) parasites form oocysts of normal size and number but they fail to generate sporozoites. This phenotype resembles to that of CS (–) parasites (Menard *et al.*, 1997), suggesting that loss of CS protein in AP2-Sp (–) parasites could be the cause of the phenotype. However, the possibility cannot be excluded that other genes involved in sporozoite formation were also regulated by AP2-Sp and that the reduced expression of these genes contributed to the phenotype. Indeed, expression of AP2-Sp starts 5 or 6 days before sporozoite budding, therefore a set of genes encoding cytoskeletal proteins, including those necessary for apical complex formation, could be under the control of AP2-Sp. In a previous paper (Yuda *et al.*, 2009), we reported that *AP2-O* (–) parasites could not form ookinetes of normal elongated shape, which suggested that AP2-O controls genes that participate in the morphogenesis of the invasive stage. Considering the analogous role of AP2-Sp and AP2-O in the respective motile stages it is possible that AP2-Sp regulates a group of genes necessary for formation of the sporozoite.

The chimeric TF induced several sporozoite-specific genes in ookinetes. ChIP-qPCR assays demonstrated that the chimeric TF activated these genes by directly binding to their promoter regions. This indicated that AP2-Sp is the *trans*-factor that interacts with the *cis*-elements. In this assay, however, the expression levels of the induced genes were not as high as those of the original ookinete-specific genes (data not shown) and significant induction was not observed in many genes, including *MAEBL*, *UIS3* and *TRAP*. It remains unclear

why this expression system did not work well on these promoters, but it is possible that co-activators of AP2-Sp, which would not be expressed in the ookinete, might be required for full activation of these promoters. Although further improvement may be required, this system could be a useful tool to determine target genes of AP2-family TFs. On the other hand, the results of the ChIP-qPCR assays suggested that the proximal promoter regions of sporozoite-specific genes are readily accessible in the ookinete stage where these genes are not primarily expressed.

Our study has demonstrated that AP2-Sp plays a central role in stage-specific gene expression in sporozoites and that *cis*-acting motifs in the proximal promoter region determine gene expression in this stage. Because the eight-base binding sequences for AP2-Sp are rarely found in the genome, these elements could mark sporozoite-specific genes on the genome. The present findings should pave the way for predicting genes expressed in this stage, based solely on genome sequence.

Experimental procedures

Parasite preparations

Female BALB/c mice (6–10 weeks old, Japan SLC, Hamamatsu, Japan) were infected with *P. berghei* ANKA strain as described previously (Yuda *et al.*, 2009). Oocyst sporozoites and salivary gland sporozoites were harvested 14 and 24 days after an infective blood meal respectively. For nuclear staining of oocysts, mosquitoes were dissected 7, 10 and 14 days after an infective blood meal, and their midguts were stained with Hoechst 34580 (Molecular Probes, Eugene, OR, USA) (0.2 μg ml^{-1} PBS final concentration) for 10 min at RT. Ookinete culture was performed as described previously (Yuda *et al.*, 2009).

Preparation of GFP-tagged AP2-Sp expressing parasites

For the targeted insertion construct (Fig. 1A), a DNA fragment containing the 3′ part of the AP2-Sp coding region was amplified by PCR, using genomic DNA as a template, and inserted into the XhoI/NheI site of the construct in frame with the GFP gene. The downstream region of the AP2-Sp gene was also amplified by PCR and inserted into the pBluescript BamHI/NotI site. Plasmids containing the construct were digested with XhoI and NotI and then used for transfection. The PCR primer pairs used for preparing the construct and Southern hybridization probe are listed in Table S5.

Targeted disruption of the AP2-Sp *gene*

The targeting construct was prepared by PCR using essentially the same procedure as described previously (Yuda *et al.*, 2009). The PCR primer pairs used for preparing the targeting construct and Southern hybridization probe are listed in Table S5.

Electrophoretic mobility-shift assays

The AP2 domain of AP2-SP was produced as a glutathione S–transferase fusion protein using the GST Gene Fusion System (Amersham Bioscience, Tokyo, Japan) essentially as described previously (Yuda *et al.*, 2009). Briefly, the coding regions were amplified from *P. berghei* genomic DNA with the primer set: 5′-CGGGATCCGCCTTTAGGGTATTTGATGT AGAC-3′ and 5′-CCGCTCGAGTTAATACTTTAGTTTCATCA TTTCGC-3′ for the AP2 domain with AT-hook region (amino acid residues 144–248) and with the primer set: 5′-CGGGATCCGCCTTTAGGGTATTTGATGTAGAC-3′ and 5′-CCGCTCGAGTTAATACTTTAGTTTCATCATTTCGC-3′ for the AP2 domain without AT-hook region (amino acid residues 157–248). Probes were prepared by PCR with 5′-biotinylated primers using the cloned promoter region of the *MAEBL* gene as template. The primer pairs used were 5′-TAAAAA TGTAAAGCATTTGAATTAAGAACC-3′ and 5′-GATGTATTT TTTGTGTAGAAAAACTGAAGG-3′. Short double-strand oligonucleotide probes were prepared from synthetic 5′-biotinylated oligonucleotides. The original oligonucleotide sequence was 5′-TAATATTATTATGCATGCATTCTTATAAG-3′. EMSA was performed as described previously (Yuda *et al.*, 2009).

Reporter assays with P. berghei *centromere plasmids*

Reporter assays were performed with the *P. berghei* centromere plasmid, pCen-GFP and pCen-Luc (Fig. S3). The upstream region of the *MAEBL* or *SPECT2* gene was inserted into the EcoRV/BamHI site, upstream of the GFP gene of pCen-GFP. For luciferase assay, the upstream promoter region was inserted into the KpnI/XhoI site upstream of the luciferase gene in pCen-Luc. The PCR primer pairs used for amplification of the upstream regions are listed in Table S6. Transfection and sporozoite preparations were performed as described previously (Yuda *et al.*, 2009). The rate of GFP-positive parasites was calculated in each sporozoite preparation. Luciferase activity was measured using 10 000 sporozoites with the Luciferase Assay System (Promega Corp., Madison, WI, USA) and normalized to rates of GFP-positive parasites.

Preparation of mutant parasites expressing AP2-O with the AP2 domain of AP2-Sp (AP2-O::Sp parasites and AP2-O::Sp::GFP parasites)

The targeted insertion construct for AP2-O::Sp parasites was prepared as follows. Part of the AP2-O coding region, just upstream of the AP2 domain, was amplified by PCR and ligated in frame to a DNA fragment encoding the AP2 domain of AP2-SP. This fragment was inserted into the XhoI/BglII site of the targeted insertion construct for AP2-O::GFP (Fig. 4A) in place of the 3′ part of the AP2-Sp coding region and the GFP gene. To prepare the targeted insertion construct for AP2-O::Sp::GFP parasites, the same fragment with XhoI/NheI

sites at the termini was inserted into the XhoI/NheI site of the targeted insertion construct for AP2-O::GFP, in frame with the GFP gene. Plasmids containing these constructs were separated from plasmid backbone by digestion with XhoI and NotI and then used for transfection. The PCR primer pairs used for preparing the targeted insertion constructs and Southern hybridization probe are listed in Table S5.

DNA microarray analysis

Ookinetes were cultured for 12 h. Five biologically independent samples were prepared from AP2-O::Sp and *AP2-O* (–) parasites. *AP2-O* (–) parasites were used as controls. Extraction of total RNA and the following microarray analyses were performed using the same procedure as described in Yuda *et al.*, (2009). Genes that increased more than threefold compared with *AP2-O* (–) parasites, for at least two probes, were selected as being induced in AP2-O::Sp parasites. From the selected genes, those having no orthologues in *P. falciparum* were excluded, because such genes are usually located in the subtelomeric regions and belong to multigene families such as the bir gene family. Microarray data have been submitted to Gene Expression Omnibus (GEO) under Accession No. GSE18910.

ChIP-quantitative PCR assays

ChIP was performed using essentially the same procedure as described previously (Yuda *et al.*, 2009). DNA fragments obtained by IP were analysed by real-time PCR using an iCycler iQ Real-Time Detection System (Bio-Rad, Hercules, CA, USA) with the primers listed in Table S7.

Acknowledgements

This work was supported by the Ministry of Education, Science, Culture, and Sports of Japan (Grant 20249023, 21022019 and 21659105 to M.Y., Grant 21022032 and 21790406 to S.I. and Grant 21790403 to I.K.) and by the Ministry of Health, Labor, and Welfare (Research Grant for Research on Emerging and Re-emerging Infectious Diseases to H.K.).

References

Aly, A.S., and Matuschewski, K. (2005) A malarial cysteine protease is necessary for Plasmodium sporozoite egress from oocysts. *J Exp Med* **202:** 225–230.

Amino, R., Giovannini, D., Thiberge, S., Gueirard, P., Boisson, B., Dubremetz, J.F., *et al.* (2008) Host cell traversal is important for progression of the malaria parasite through the dermis to the liver. *Cell Host Microbe* **3:** 88–96.

Balaji, S., Babu, M.M., Iyer, L.M., and Aravind, L. (2005) Discovery of the principal specific transcription factors of Apicomplexa and their implication for the evolution of the AP2-integrase DNA binding domains. *Nucleic Acids Res* **33:** 3994–4006.

De Silva, E.K., Gehrke, A.R., Olszewski, K., Leon, I., Chahal, J.S., Bulyk, M.L., and Llinas, M. (2008) Specific DNA-binding by apicomplexan AP2 transcription factors. *Proc Natl Acad Sci USA* **105:** 8393–8398.

Dessens, J.T., Siden-Kiamos, I., Mendoza, J., Mahairaki, V., Khater, E., Vlachou, D., *et al.* (2003) SOAP, a novel malaria ookinete protein involved in mosquito midgut invasion and oocyst development. *Mol Microbiol* **49:** 319–329.

Ishino, T., Yano, K., Chinzei, Y., and Yuda, M. (2004) Cell-passage activity is required for the malarial parasite to cross the liver sinusoidal cell layer. *PLoS Biol* **2:** E4.

Ishino, T., Chinzei, Y., and Yuda, M. (2005) A Plasmodium sporozoite protein with a membrane attack complex domain is required for breaching the liver sinusoidal cell layer prior to hepatocyte infection. *Cell Microbiol* **7:** 199–208.

Jofuku, K.D., den Boer, B.G., Van Montagu, M., and Okamuro, J.K. (1994) Control of Arabidopsis flower and seed development by the homeotic gene APETALA2. *Plant Cell* **6:** 1211–1225.

Kariu, T., Yuda, M., Yano, K., and Chinzei, Y. (2002) MAEBL is essential for malarial sporozoite infection of the mosquito salivary gland. *J Exp Med* **195:** 1317–1323.

Matuschewski, K., Ross, J., Brown, S.M., Kaiser, K., Nussenzweig, V., and Kappe, S.H. (2002) Infectivity-associated changes in the transcriptional repertoire of the malaria parasite sporozoite stage. *J Biol Chem* **277:** 41948–41953.

Menard, R., Sultan, A.A., Cortes, C., Altszuler, R., van Dijk, M.R., Janse, C.J., *et al.* (1997) Circumsporozoite protein is required for development of malaria sporozoites in mosquitoes. *Nature* **385:** 336–340.

Moreira, C.K., Templeton, T.J., Lavazec, C., Hayward, R.E., Hobbs, C.V., Kroeze, H., *et al.* (2008) The Plasmodium TRAP/MIC2 family member, TRAP-like protein (TLP), is involved in tissue traversal by sporozoites. *Cell Microbiol* **10:** 1505–1516.

Mueller, A.K., Labaied, M., Kappe, S.H., and Matuschewski, K. (2005) Genetically modified Plasmodium parasites as a protective experimental malaria vaccine. *Nature* **433:** 164–167.

Young, J.A., Johnson, J.R., Benner, C., Yan, S.F., Chen, K., Le Roch, K.G., *et al.* (2008) In silico discovery of transcription regulatory elements in *Plasmodium falciparum*. *BMC Genomics* **9:** 70.

Yuda, M., Iwanaga, S., Shigenobu, S., Mair, G.R., Janse, C.J., Waters, A.P., *et al.* (2009) Identification of a transcription factor in the mosquito-invasive stage of malaria parasites. *Mol Microbiol* **71:** 1402–1414.

Supporting information

Additional supporting information may be found in the online version of this article.

Please note: Wiley-Blackwell are not responsible for the content or functionality of any supporting materials supplied by the authors. Any queries (other than missing material) should be directed to the corresponding author for the article.

nature medicine

Human P-selectin glycoprotein ligand-1 is a functional receptor for enterovirus 71

Yorihiro Nishimura[1], Masayuki Shimojima[2], Yoshio Tano[1,3], Tatsuo Miyamura[1], Takaji Wakita[1] & Hiroyuki Shimizu[1]

Enterovirus 71 (EV71) is a major causative agent of hand, foot and mouth disease (HFMD), a common febrile disease occurring mainly in young children. Although clinical manifestations of HFMD are usually mild and self limiting, a severe EV71 outbreak can lead to a diverse array of neurological diseases. Identification of the specific cellular receptors is crucial for elucidating the mechanism of early virus-host interactions and the pathogenesis of enteroviruses[1]. Here we identify human P-selectin glycoprotein ligand-1 (PSGL-1; CD162), a sialomucin membrane protein expressed on leukocytes that has a major role in early stages of inflammation[2–4], as a functional receptor for EV71 using an expression cloning method by panning[5]. The N-terminal region of PSGL-1 binds specifically to EV71. Stable PSGL-1 expression allowed EV71 entry and replication, and development of cytopathic effects in nonsusceptible mouse L929 cells. Five out of eight EV71 strains bound soluble PSGL-1 and used intact PSGL-1 as the primary receptor for infection of Jurkat T cells. Three other EV71 strains did not use PSGL-1, suggesting the presence of strain-specific replication of EV71 in leukocytes. EV71 replicated in nonleukocyte cell lines in a PSGL-1–independent manner, indicating the presence of alternative receptor(s) for EV71. The identification of PSGL-1 as a receptor for EV71 sheds new light on a role for PSGL-1–positive leukocytes in cell tropism and pathogenesis during the course of HFMD and other EV71-mediated diseases.

EV71 and coxsackievirus A16 (CVA16) belong to the human enterovirus species A of the genus *Enterovirus*[6] and are the major causative agents of HFMD. EV71 may cause various neurological diseases, such as aseptic meningitis, acute flaccid paralysis and fatal neurogenic pulmonary edema. Severe EV71 outbreaks have been reported periodically throughout the world, representing a major public health concern, particularly in the Asia-Pacific region[7–9]. During large outbreaks of EV71, individuals with severe EV71-associated encephalitis and neurogenic pulmonary edema showed a marked depletion of T cells and high levels of proinflammatory cytokines[10,11]. Because of this T cell involvement, we generated a retroviral complementary DNA (cDNA) library from Jurkat T cells that are susceptible to EV71 infection[12] and used it for expression cloning[5] to identify a receptor that specifically binds EV71 virions (EV71-1095 strain, **Supplementary Table 1**). Transduction of mouse myeloma P3X63Ag8U.1 (P3U1) cells with the Jurkat cDNA library resulted in the formation of four colonies that bound EV71-1095–coated dishes, all of which encoded human PSGL-1 (*SELPLG*) (**Fig. 1a** and **Supplementary Fig. 1**).

To confirm the specific binding of PSGL-1 to EV71-1095, we used 293T cells, which express undetectable amounts of endogenous PSGL-1. Transient expression of human PSGL-1 on 293T cells markedly increased the binding of EV71-1095 to 293T cells (**Fig. 1b**); however, expression of control ligands (sialomucin proteins CD34 and CD43) and mouse Psgl-1 did not (**Supplementary Fig. 2**). To identify the region of human PSGL-1 that is important for EV71 binding, we first constructed a chimeric PSGL-1 (hmPSGL-1) containing amino acids 1–61 of the human PSGL-1 followed by amino acids 63–397 of mouse Psgl-1 (**Supplementary Fig. 3a,b**). EV71-1095 bound hmPSGL-1 expressed on 293T cells (**Supplementary Fig. 3c**). To confirm this finding, we examined whether monoclonal antibodies (mAbs) recognizing PSGL-1 (KPL1 (refs. 13,14) and PL2 (ref. 15); **Fig. 1a**) block the PSGL-1–EV71 interaction. KPL1, which blocks P-selectin binding to PSGL-1 (ref. 13), inhibited EV71-1095 binding to 293T cells transiently expressing PSGL-1 in a dose-dependent manner; however, PL2, which does not block binding to P-selectin, did not (**Fig. 1c**). These findings suggest that the N-terminal region (amino acids 42–61) of human PSGL-1 is crucial for interactions with EV71-1095.

To test whether PSGL-1 is involved in the later steps of viral entry after binding to cells, we used mouse cells that do not support EV71 infection. Mouse myeloma P3U1 cells expressing human PSGL-1 did not support efficient EV71 replication (data not shown). Therefore, we obtained an L929 cell clone (L-PSGL-1.1) that stably expresses high amounts of human PSGL-1 (**Fig. 2a**). L-PSGL-1.1 cells showed a cytopathic effect 4 d after infection, and we detected EV71 antigen by immunofluorescence in the infected L-PSGL-1.1 cells (**Fig. 2b**). The development of cytopathic effect and detection of viral antigens induced by EV71-1095 infection was markedly inhibited by KPL1 (**Fig. 2b**), but not by PL2 (data not shown), as were the replication kinetics of EV71-1095 in infected L-PSGL-1.1 cells (**Fig. 2c,d**),

[1]Department of Virology II, National Institute of Infectious Diseases, Musashimurayama-shi, Tokyo, Japan. [2]Division of Virology, Department of Microbiology and Immunology, Institute of Medical Science, University of Tokyo, Minato-ku, Tokyo, Japan. [3]Present address: Japan Poliomyelitis Research Institute, Higashimurayama-shi, Tokyo, Japan. Correspondence should be addressed to H.S. (hshimizu@nih.go.jp).

Received 2 December 2008; accepted 6 April 2009; published online 21 June 2009; doi:10.1038/nm.1961

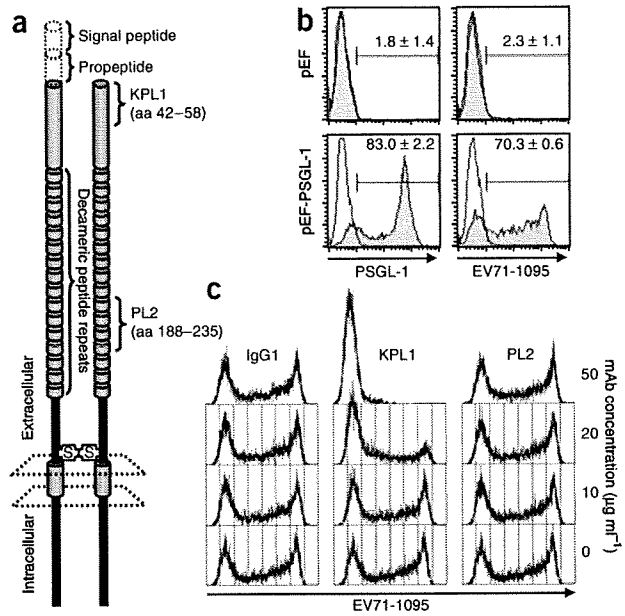

Figure 1 EV71-1095 binds human PSGL-1 expressed on 293T cells. (**a**) Schematic structure of human PSGL-1. The binding sites of PSGL-1–specific mAbs (KPL1 (ref. 14) and PL2 (ref. 15)) are indicated. aa, amino acids. (**b**) Flow cytometric analysis of 293T cells transfected with pEF-PSGL-1 or pEF (a control plasmid). Left, shaded and open areas represent staining with KPL1 mAb and isotype control, respectively. Right, shaded and open areas represent EV71-1095 binding assay and binding control with the mock-infected culture supernatant, respectively. The percentage of PSGL-1– or EV71-positive cells is indicated (mean ± s.d., $n = 3$). (**c**) EV71-1095 binding inhibition assay by flow cytometry. Dose-dependent inhibition of EV71-1095 binding to 293T cells transiently expressing PSGL-1 by mAb.

indicating PSGL-1–dependent EV71 replication in these cells. Furthermore, pretreatment of EV71-1095 with a soluble form of recombinant PSGL-1 (PSGL-1–Fc) impaired viral replication 2–4 d after viral inoculation of L-PSGL-1.1 cells (**Fig. 2e**) and RD cells (**Supplementary Table 2**) expressing undetectable PSGL-1 (data not shown), suggesting that the inhibitory effect of PSGL-1–Fc is due to either direct binding to EV71 virions or virion uncoating induced by the PSGL-1–Fc–EV71 interaction.

To elucidate the biological role of PSGL-1–dependent cell tropism of EV71-1095, we investigated the relationship between PSGL-1 expression on the cell surface (**Fig. 3a**) and replication of EV71 (**Fig. 3b**) in various cell lines (**Supplementary Table 2**). Among the four leukocyte cell lines examined, we found PSGL-1–dependent viral replication, as indicated by the reduction of viral titers in the presence of KPL1 in Jurkat T cells and U937 monocytic cells, which express large amounts of PSGL-1 on the cell surface. EV71-1095 induced a faint cytopathic effect in Jurkat T cells but no apparent cytopathic effect in the other leukocyte cell lines (data not shown). EV71-1095 replication was not affected by KPL1 in MT-2 cells and four nonleukocyte cell lines (RD, HEp-2c, SK-N-MC and Vero) that have little or no PSGL-1 expression, suggesting PSGL-1–independent replication through unidentified receptors in MT-2 and nonleukocyte cells. Taken together, these results suggest that EV71-1095 can use PSGL-1 as a functional cellular receptor in PSGL-1–positive leukocytes (**Supplementary Fig. 1a**), but it may use alternative mechanism(s) for replication in cells that have little or no PSGL-1 expression (**Supplementary Fig. 1b**).

Although the association of a specific genogroup with severe neurological diseases has not been identified through molecular epidemiological analyses of previous and recent EV71 isolates (genogroups A, B and C)[9,16], *in vitro* and *in vivo* phenotypes may be associated with certain amino acid determinants of EV71. Using eight representative EV71 strains (**Supplementary Table 1**), we investigated the strain specificity of EV71 and PSGL-1 use. We first examined the direct biochemical interaction between EV71 strains and PSGL-1–Fc by co-immunoprecipitation. The VP1 proteins of the SK-EV006, C7/Osaka, KED005, 1095 and 75-Yamagata strains of EV71 immunoprecipitated with PSGL-1–Fc (**Fig. 4a**). In contrast, the VP1 proteins of the BrCr, Nagoya and 02363 strains of EV71 did not immunoprecipitate with PSGL-1–Fc (**Fig. 4a**). Thus, these EV71 strains can be classified into two distinct phenotypes according to their PSGL-1–binding capability, regardless of genogroup: five PSGL-1–binding strains (EV71-PB; SK-EV006 (genogroup B3), C7/Osaka (B4), KED005 (C1), 1095 (C2) and 75-Yamagata (C4)) and three PSGL-1–nonbinding strains (EV71–non-PB; BrCr (A), Nagoya (B1) and 02363 (C1)). We then tested the PSGL-1–dependent replication competence of EV71-PB and EV71–non-PB strains in Jurkat T cells

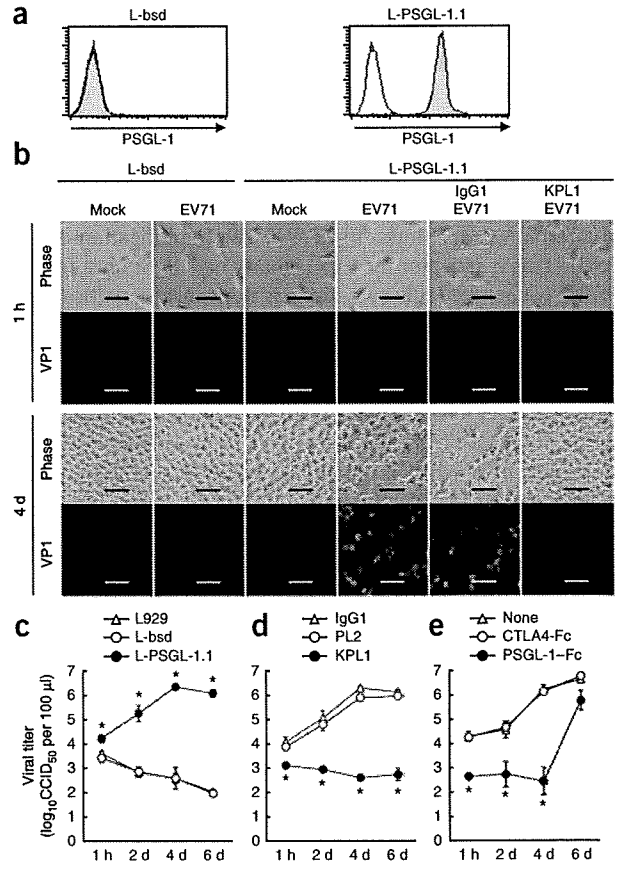

Figure 2 Stable expression of human PSGL-1 on mouse L929 cells permits infection by EV71-1095. (**a**) PSGL-1 expression on L-PSGL-1.1 and L-bsd (PSGL-1 negative control) cells, as measured by flow cytometry. (**b**) Development of cytopathic effect (Phase) and EV71 antigens by immunofluorescence (VP1). Scale bars, 100 μm. (**c**) Replication kinetics of EV71-1095 in L-PSGL-1.1 and PSGL-1–negative cells. (**d**) Replication kinetics of EV71-1095 in L-PSGL-1.1 cells in the presence of PSGL-1–specific (KPL1 and PL2) and control mAbs. (**e**) Replication kinetics of EV71-1095 in L-PSGL-1.1 cells after treatment with soluble PSGL-1. Viral titers and error bars are indicated as the means ± s.d. of triplicate analyses. Asterisks indicate $P < 0.01$ compared to the two controls.

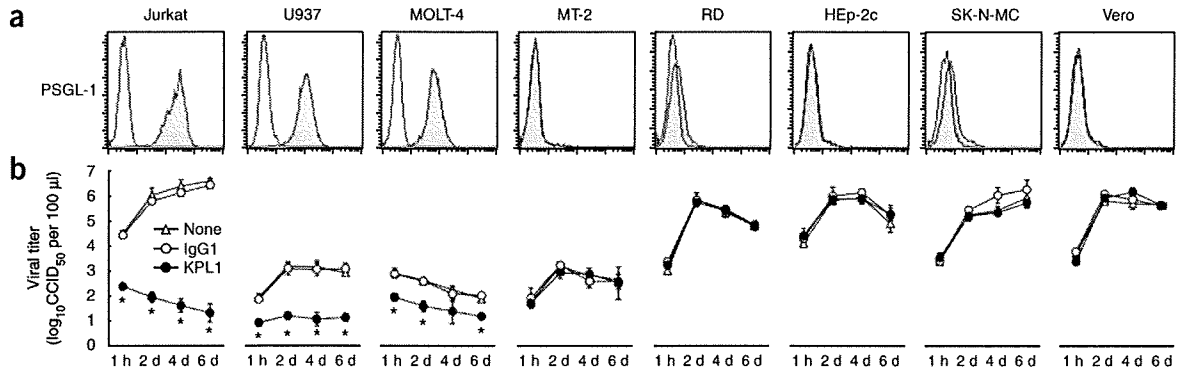

Figure 3 PSGL-1 expression and EV71-1095 replication kinetics in leukocyte and nonleukocyte cell lines. (**a**) PSGL-1 expression on the cell surface, as measured by flow cytometry. The shaded and open areas represent staining with PSGL-1–specific mAb (KPL1) and isotype control, respectively. (**b**) EV71-1095 replication kinetics in the presence of KPL1 and control mAbs. The titers and error bars are the means ± s.d. of triplicate analyses. Asterisks indicate $P < 0.01$ compared to the two controls.

(**Fig. 4b**). All five EV71-PB strains replicated in Jurkat T cells in a PSGL-1–dependent manner, as indicated by the reduction of viral titers in the presence of KPL1 at 4 d after inoculation (**Fig. 4b**). Among the three EV71–non-PB strains, two (Nagoya and 02363) replicated in Jurkat T cells in a PSGL-1–independent manner, and the BrCr strain replicated poorly (**Fig. 4b**). These data indicate that EV71-PB strains use PSGL-1 as the primary and functional receptor for infection of Jurkat T cells (**Supplementary Fig. 1a**), whereas some of the EV71–non-PB strains may use unidentified receptors for viral replication even in PSGL-1–positive T lymphocytes (**Supplementary Fig. 1c**). Although the KED005 and 02363 strains (genogroup C1) show distinct differences in their PSGL-1–binding phenotypes, only four amino acids (Ile55 of VP3 and Lys98, Glu145 and Ile262 of VP1 for the EV71-02363 strain) are different in the proteins comprising the entire capsid region of these two strains, suggesting that a few amino acid determinants in the capsid proteins are fully responsible for the phenotype (**Fig. 4**). Among the four amino acid differences, Glu145 of VP1 may be exposed on a surface-exposed loop in the capsid VP1 protein, and this has been identified as a major virulence determinant in mouse models[17,18].

We next investigated PSGL-1–dependent replication of the prototype CVA16-G10 strain. This strain replicated in L-PSGL-1.1 cells but not in L-bsd cells (a PSGL-1–negative control), and virus replication in L-PSGL-1.1 cells was inhibited by KPL1 (**Supplementary Fig. 4a,b**). The CVA16-G10 strain used PSGL-1 to infect L-PSGL-1.1 cells but not Jurkat T cells (**Supplementary Fig. 4c**), suggesting that CVA16-G10 represents a strain that uses an alternative entry mechanism via unidentified functional receptors for infection of Jurkat T cells.

PSGL-1 expressed on leukocytes has a crucial role in the tethering and rolling of leukocytes during recruitment of cells from blood vessels to the sites of acute inflammation upon stimulation by infection[2–4]. The tissue expression of PSGL-1 is primarily restricted to hematopoietic myeloid, lymphoid and dendritic lineages and to platelets. However, PSGL-1 is also expressed on the dendritic cells of lymph nodes and on macrophages in the intestinal mucosa[2], which could be the primary site of EV71 replication after viral ingestion. During the viremic phase of infection, a variety of circulating leukocytes expressing PSGL-1 may be responsible for the *in vivo* replication of EV71 (ref. 19) and subsequent EV71-induced apoptosis in the infected cells[12,20], possibly resulting in the T cell depletion and changes in cytokine levels observed in severe

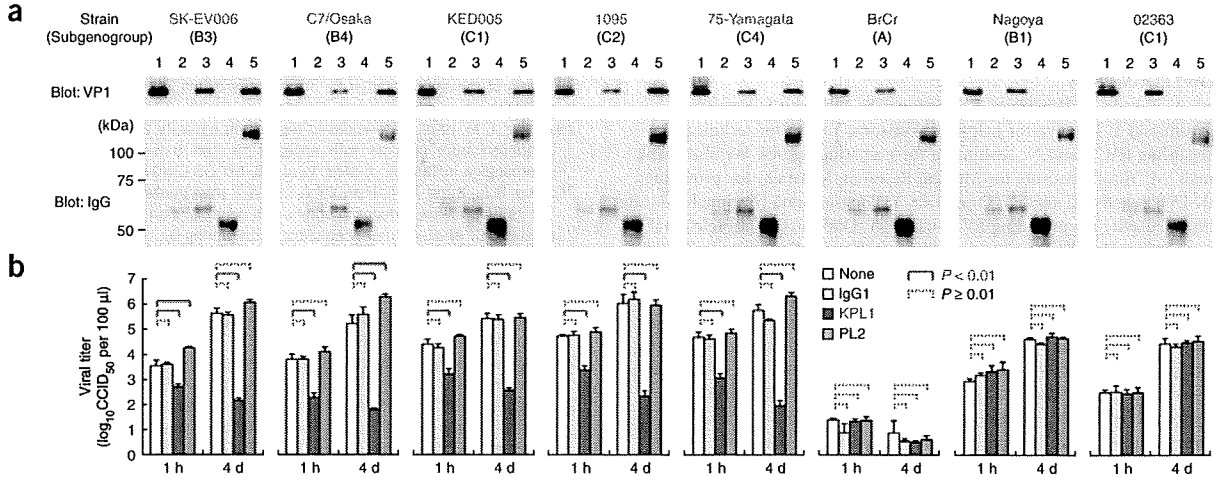

Figure 4 EV71 strain–specific binding to PSGL-1 and replication in Jurkat T cells. The strains that are EV71-PB and EV71–non-PB are indicated in red and blue, respectively. (**a**) Western blot showing the EV71 VP1 protein immunoprecipitated with PSGL-1–Fc. Concentrated viruses (lane 1) were incubated with isotype control mAb (lane 2), EV71-VP1–specific mAb (MA105, lane 3), negative control recombinant protein (CTLA4-Fc, lane 4) or PSGL-1–Fc (lane 5) and immunoprecipitated. (**b**) Viral replication in Jurkat T cells incubated with PSGL-1–specific (KPL1 and PL2) and control mAbs. Titers are expressed as the mean, and error bars indicate s.d. of triplicate analyses.

encephalitis cases with pulmonary edema[10,11]. In addition, the distribution and recruitment of PSGL-1–positive Langerhans cells and lymphocytes in inflamed skin[2] are consistent with the apparent HFMD pathogenesis associated with EV71 and CVA16 infection, which is characterized by acute skin inflammation. In this regard, our findings suggest the involvement of PSGL-1–positive inflammatory cells during the course of EV71 and CVA16 infection.

Although EV71 infects neurons and causes acute brainstem encephalitis, paralysis or both in humans[21,22] and experimental animals[17,23–25], PSGL-1 is apparently not expressed in the adult human brain[2]. Consistent with this observation, we have shown that EV71-1095 may also use PSGL-1–independent mechanism(s) for replication in nonleukocyte cells, including SK-N-MC neuroblastoma cells. Furthermore, CVA16, another causative agent of HFMD, can also use PSGL-1 as a functional receptor in L-PSGL-1.1 cells. Thus, PSGL-1–dependent viral replication is unlikely to be directly responsible for the neuronal cell apoptosis induced by EV71 (refs. 26,27). However, we cannot exclude the possible involvement of PSGL-1–positive inflammatory cells in the pathogenesis of HFMD and a variety of EV71 diseases with or without neurological manifestations.

We have shown that human PSGL-1 is a functional cellular receptor for EV71 infection. The occurrence of severe EV71 infection with a number of fatal encephalitis cases continues to be a major public health threat even now[28], but, currently, no vaccines or specific antiviral agents are available for EV71. Because soluble PSGL-1 inhibits EV71 replication, it may be a potential inhibitor of EV71-PB infection. The identification of PSGL-1 as a functional EV71 receptor on leukocytes is the first major step in elucidating EV71 pathogenesis at the molecular level. However, other EV71 and human enterovirus species A receptors on leukocyte and nonleukocyte cells may also have key implications in EV71 tropism and pathogenesis, particularly for severe central nervous system diseases. Further structural and functional analyses of interactions of EV71 with PSGL-1 and other unidentified receptors may provide new therapeutic approaches for the treatment of severe EV71 diseases.

METHODS

Methods and any associated references are available in the online version of the paper at http://www.nature.com/naturemedicine/.

Note: Supplementary information is available on the Nature Medicine website.

ACKNOWLEDGMENTS

We thank N. Takeda, S. Morikawa, Y. Matsuura, K. Moriishi, S. Koike, S. Yamayoshi and Y. Izumiya for helpful discussions; Y. Ami for technical advice regarding FACS; and N. Nishimura for preparing figures. We also thank M. Sinniah, M. Yusof (Institute for Medical Research, Malaysia) for providing EV71-SK-EV006 and KED005, N. Onnimala, Y. Pongsuwanna (National Institute of Health, Thailand) for providing EV71-02363, Y. Okuno (Osaka Prefectural Institute of Public Health) for providing EV71-C7/Osaka, K. Mizuta (Yamagata Prefectural Institute of Public Health) for providing EV71-75-Yamagata, A. Makino, Y. Tohya, H. Akashi (University of Tokyo) for providing P3U1 cells, H. Sakata (National Institute of Infectious Diseases, Japan) for providing L929 cells, and H. Shirato (National Institute of Infectious Diseases, Japan) for providing MOLT-4 and MT-2 cells. We are grateful to J. Wada for technical assistance. This work was supported by a Grant-in-Aid for Young Scientists from the Ministry of Education, Culture, Sports, Science and Technology, Japan (Y.N.). Y.N. and H.S. were supported in part by a Grant-in-Aid for Research on Emerging and Re-emerging Infectious Diseases and a Grant-in-Aid for the Promotion of Polio Eradication, from the Ministry of Health, Labour and Welfare, Japan.

AUTHOR CONTRIBUTIONS

Y.N. designed and performed experiments, analyzed data and wrote the paper; M.S. improved the expression cloning method; Y.T. prepared and characterized EV71-specific mAbs; and T.M. and T.W. analyzed data and wrote the paper. H.S. planned the project, designed experiments, analyzed data and wrote the paper. All authors discussed the results and commented on the manuscript.

Published online at http://www.nature.com/naturemedicine/
Reprints and permissions information is available online at http://npg.nature.com/reprintsandpermissions/

1. Rossmann, M.G., He, Y. & Kuhn, R.J. Picornavirus-receptor interactions. *Trends Microbiol.* **10**, 324–331 (2002).
2. Laszik, Z. *et al.* P-selectin glycoprotein ligand-1 is broadly expressed in cells of myeloid, lymphoid, and dendritic lineage and in some nonhematopoietic cells. *Blood* **88**, 3010–3021 (1996).
3. Sako, D. *et al.* Expression cloning of a functional glycoprotein ligand for P-selectin. *Cell* **75**, 1179–1186 (1993).
4. Somers, W.S., Tang, J., Shaw, G.D. & Camphausen, R.T. Insights into the molecular basis of leukocyte tethering and rolling revealed by structures of P- and E-selectin bound to SLe^X and PSGL-1. *Cell* **103**, 467–479 (2000).
5. Shimojima, M. *et al.* Usage of myeloma and panning in retrovirus-mediated expression cloning. *Anal. Biochem.* **315**, 138–140 (2003).
6. Oberste, M.S., Maher, K., Kilpatrick, D.R. & Pallansch, M.A. Molecular evolution of the human enteroviruses: correlation of serotype with VP1 sequence and application to picornavirus classification. *J. Virol.* **73**, 1941–1948 (1999).
7. Chan, L.G. *et al.* Deaths of children during an outbreak of hand, foot and mouth disease in Sarawak, Malaysia: clinical and pathological characteristics of the disease. *Clin. Infect. Dis.* **31**, 678–683 (2000).
8. Ho, M. *et al.* An epidemic of enterovirus 71 infection in Taiwan. *N. Engl. J. Med.* **341**, 929–935 (1999).
9. McMinn, P.C. An overview of the evolution of enterovirus 71 and its clinical and public health significance. *FEMS Microbiol. Rev.* **26**, 91–107 (2002).
10. Lin, T.Y., Hsia, S.H., Huang, Y.C., Wu, C.T. & Chang, L.Y. Proinflammatory cytokine reactions in enterovirus 71 infections of the central nervous system. *Clin. Infect. Dis.* **36**, 269–274 (2003).
11. Wang, S.M. *et al.* Pathogenesis of enterovirus 71 brainstem encephalitis in pediatric patients: roles of cytokines and cellular immune activation in patients with pulmonary edema. *J. Infect. Dis.* **188**, 564–570 (2003).
12. Chen, L.C. *et al.* Enterovirus 71 infection induces Fas ligand expression and apoptosis of Jurkat cells. *J. Med. Virol.* **78**, 780–786 (2006).
13. Snapp, K.R. *et al.* A novel P-selectin glycoprotein ligand-1 monoclonal antibody recognizes an epitope within the tyrosine sulfate motif of human PSGL-1 and blocks recognition of both P- and L-selectin. *Blood* **91**, 154–164 (1998).
14. Thatte, A. *et al.* Binding of function-blocking mAbs to mouse and human P-selectin glycoprotein ligand-1 peptides with and without tyrosine sulfation. *J. Leukoc. Biol.* **72**, 470–477 (2002).
15. Li, F. *et al.* Visualization of P-selectin glycoprotein ligand-1 as a highly extended molecule and mapping of protein epitopes for monoclonal antibodies. *J. Biol. Chem.* **271**, 6342–6348 (1996).
16. Brown, B.A., Oberste, M.S., Alexander, J.P. Jr., Kennett, M.L. & Pallansch, M.A. Molecular epidemiology and evolution of enterovirus 71 strains isolated from 1970 to 1998. *J. Virol.* **73**, 9969–9975 (1999).
17. Arita, M., Ami, Y., Wakita, T. & Shimizu, H. Cooperative effect of the attenuation determinants derived from poliovirus Sabin 1 strain is essential for attenuation of enterovirus 71 in the NOD/SCID mouse infection model. *J. Virol.* **82**, 1787–1797 (2008).
18. Chua, B.H., Phuektes, P., Sanders, S.A., Nicholls, P.K. & McMinn, P.C. The molecular basis of mouse adaptation by human enterovirus 71. *J. Gen. Virol.* **89**, 1622–1632 (2008).
19. Kung, C.M. *et al.* Differences in replication capacity between enterovirus 71 isolates obtained from patients with encephalitis and those obtained from patients with herpangina in Taiwan. *J. Med. Virol.* **79**, 60–68 (2007).
20. Kuo, R.L., Kung, S.H., Hsu, Y.Y. & Liu, W.T. Infection with enterovirus 71 or expression of its 2A protease induces apoptotic cell death. *J. Gen. Virol.* **83**, 1367–1376 (2002).
21. Hsueh, C. *et al.* Acute encephalomyelitis during an outbreak of enterovirus type 71 infection in Taiwan: report of an autopsy case with pathologic, immunofluorescence and molecular studies. *Mod. Pathol.* **13**, 1200–1205 (2000).
22. Wong, K.T. *et al.* The distribution of inflammation and virus in human enterovirus 71 encephalomyelitis suggests possible viral spread by neural pathways. *J. Neuropathol. Exp. Neurol.* **67**, 162–169 (2008).
23. Nagata, N. *et al.* Pyramidal and extrapyramidal involvement in experimental infection of cynomolgus monkeys with enterovirus 71. *J. Med. Virol.* **67**, 207–216 (2002).
24. Nagata, N. *et al.* Differential localization of neurons susceptible to enterovirus 71 and poliovirus type 1 in the central nervous system of cynomolgus monkeys after intravenous inoculation. *J. Gen. Virol.* **85**, 2981–2989 (2004).
25. Ong, K.C. *et al.* Pathologic characterization of a murine model of human enterovirus 71 encephalomyelitis. *J. Neuropathol. Exp. Neurol.* **67**, 532–542 (2008).
26. Chang, S.C., Lin, J.Y., Lo, L.Y.C., Li, M.L. & Shih, S.R. Diverse apoptotic pathways in enterovirus 71–infected cells. *J. Neurovirol.* **10**, 338–349 (2004).
27. Chen, C.S. *et al.* Retrograde axonal transport: a major transmission route of enterovirus 71 in mice. *J. Virol.* **81**, 8996–9003 (2007).
28. World Health Organization. Outbreak news. Enterovirus, China. *Wkly. Epidemiol. Rec.* **83**, 169–170 (2008).

ONLINE METHODS

Cells. L929 cells were generously provided by H. Sakata P3U1 cells were generously provided by H. Akashi. 293T cells were generously provided by Y. Matsuura. GP2-293 cells were obtained from Clontech. Jurkat cells were obtained from Riken Cell Bank. U937 cells were obtained from the Japanese Collection of Research Biosources. MOLT-4 and MT-2 cells were generously provided by H. Shirato. RD cells were obtained from the US Centers for Disease Control. HEp-2 cells were obtained from the Victorian Infectious Diseases Reference Laboratory. SK-N-MC cells were obtained from DS Pharma Biomedical. Vero cells were obtained from Japan Poliomyelitis Research Institute. We cultured L929, 293T and GP2-293 cells in DMEM (Sigma) supplemented with 10% FCS. We maintained P3U1, Jurkat, U937, MOLT-4 and MT-2 cells in RPMI-1640 medium (Sigma) with 10% FCS. We maintained RD, HEp-2c, SK-N-MC and Vero cells in Eagle's minimal essential medium (Nissui) supplemented with 10% FCS.

Viruses. We propagated all EV71 strains (**Supplementary Table 1**) in RD or Vero cells. Because some of the strains produced diffuse plaques on RD cells, we determined the viral titers by a microtitration assay using 96-well plates and RD cells as previously described[23]. Briefly, we used ten wells for each viral dilution and expressed the viral titers as 50% cell culture infectious dose ($CCID_{50}$).

Monoclonal antibodies and recombinant proteins. We generated the EV71-specific mAbs MA105 (mouse IgG2b) and MA35 (mouse IgG2a) from mice immunized with EV71-1095 (Y. Tano *et al.*, unpublished data). We purchased the EV71-specific mAb 10F0 from Biogenesis. We purchased the mAbs to human CD34 (clone 563), human CD43 (L60), human PSGL-1 (KPL1), and mouse Psgl-1 (4RA10) from BD Biosciences, and we purchased human PSGL-1–specific mAb PL2 from Beckman-Coulter. For negative controls, we purchased human (MOPC-21) and rat IgG1 (R3-34) and human IgG2b (27-35) from BD Biosciences. We used NaN_3-free mAbs, MOPC-21 (BioLegend) and NCG01 (Lab Vision) in cell culture as negative controls. We purchased soluble recombinant forms of human proteins fused to the Fc region of human IgG1 (PSGL-1–Fc and cytotoxic T lymphocyte antigen-4–Fc) from R&D Systems.

Preparation of EV71-1095–coated dishes and selection of Jurkat T cell clones. We incubated a polystyrene Petri dish (Ina-optika) with 10 μg ml^{-1} MA35 in 10 ml of 50 mM Tris-HCl (pH 9.4) at 4 °C overnight. We rinsed the dishes twice with PBS containing 2% FCS (PBS-2FCS) and blocked them with PBS-2FCS at 25 °C for 30 min. We then applied EV71-1095 (10 ml, $1 \times 10^{8.6}$ $CCID_{50}$ ml^{-1}) to the MA35-coated dishes and incubated at 25 °C for 30 min. We replaced the supernatant with a fresh viral preparation, and we repeated replacing the supernatant three times. We fixed the dishes with a viral preparation containing 1% paraformaldehyde for 30 min at 25 °C. Finally, we washed the dishes with PBS-2FCS five times and used them for selection and expression cloning.

We selected Jurkat T cell clones that expressed high levels of EV71-binding molecules on the cell surface with the panning method with EV71-1095–coated dishes. We added Jurkat T cells to the EV71-coated dishes in RPMI-1640 medium and incubated them at 4 °C for 90 min. We removed nonadherent cells by washing with RPMI-1640 medium, and we cultured the adherent cells for a week. We used the Jurkat T cell colonies on the EV71-coated dishes for preparation of the cDNA library.

Retroviral cDNA library. Using the Jurkat T cell colonies on the EV71-coated dishes, we prepared a retroviral cDNA library as previously described[29] with minor modifications. We used the Pantropic Retroviral Expression System (Clontech) to prepare vesicular stomatitis virus G protein–pseudotyped retroviruses. We ligated the Jurkat cDNA with the EcoRI adaptor and cloned it into the EcoRI site of the pLIB retroviral vector (Clontech). We transfected the pLIB plasmid along with a vesicular stomatitis virus G protein expression plasmid into GP2-293 cells with Lipofectamine 2000 (Invitrogen). We harvested the culture supernatant 2 d after transfection and used it to infect P3U1 cells.

Expression cloning of the EV71-binding receptor. We preformed retrovirus-mediated expression cloning using EV71-coated dishes and P3U1 cells as described previously[5]. We isolated genomic DNA from each P3U1 cell colony bound to the EV71-coated dishes, subjected it to PCR amplification with pLIB-specific primers and sequenced the amplification product.

Expression plasmids. We cloned the cDNAs encoding human *SELPLG*, *CD34*, *SPN* and mouse *Selplg* into pEF6-Flag-3S to produce pEF-PSGL-1, pEF-CD34, pEF-CD43 and pEF-mPsgl-1, respectively. For hmPSGL-1 expression, we constructed chimeric *SELPLG* cDNA by PCR and cloned it into pEF6-Flag-3S. The primers used for cDNA cloning and chimeric protein construction and mutation are shown in **Supplementary Tables 3** and **4**. More details are provided in the **Supplementary Methods**.

Detection of cell surface molecules by flow cytometry. We washed cells once with flow cytometry buffer (PBS supplemented with 2 mM EDTA, 2% FCS and 0.1% NaN_3) and incubated them with mAb on ice for 30 min. After washing with flow cytometry buffer, we incubated the cells with secondary antibodies conjugated to Alexa Fluor 488 (Invitrogen). We washed and analyzed the cells by FACSCalibur (BD Biosciences).

EV71-binding assay by flow cytometry. We collected 293T cells 24 h after transfection with expression plasmids, washed them once with flow cytometry buffer and incubated them with the EV71-1095 preparation (1×10^7 $CCID_{50}$) supplemented with 0.1% NaN_3 or concentrated viruses (containing 0.5 μg of VP1 protein) per 50 μl flow cytometry buffer. In the binding inhibition assay with mAbs, we treated cells with mAb for 30 min on ice before exposing them to the virus. We washed the cells and stained them with Alexa Fluor 488–conjugated MA105, washed them and then analyzed them by FACSCalibur.

Establishment of the L-PSGL-1.1 cell line. To establish a mouse L929 cell line expressing human PSGL-1, we transfected L929 cells with pEF-PSGL-1 and selected stable transfectants with 5 μg ml^{-1} blasticidin S HCl (Invitrogen). Through a limiting dilution of the various cell colonies, we selected three of the 16 cell lines on the basis of high PSGL-1 expression. Finally, we established L-PSGL-1.1 as the single cell clone that supported the most efficient EV71-1095 replication. As a PSGL-1–negative control, we also established an L-bsd cell line by transfecting L929 cells with pEF6-Flag-3S followed by selection with 5 μg ml^{-1} blasticidin.

Immunofluorescence microscopy. We fixed cells with 4% paraformaldehyde in PBS for 30 min at 25 °C, washed them, permeabilized them with PBS containing 1% Triton X-100 for 10 min at 25 °C, blocked them with PBS containing 1% BSA for 10 min at 25 °C and incubated them with VP1-specific mAb 10F0 labeled with Alexa Fluor 488 for 30 min at 37 °C. After a final wash, we analyzed the cells with a fluorescence microscope (Keyence).

Immunoprecipitation and western blotting. We diluted concentrated viruses (0.5 μg VP1 protein) in 300 μl of immunoprecipitation buffer (20 mM Tris-Cl, 135 mM NaCl, 1% Triton X-100 and 10% glycerol; pH 7.4) and incubated them with 1 μg of mAb or chimeric proteins for 2 h at 4 °C. We added Dynabeads Protein G (Invitrogen) and incubated the mixture for an additional 2 h. We washed the beads and subjected the immunoprecipitates to 12.5% SDS-PAGE. For western blotting, we transferred the proteins onto nitrocellulose membranes and blotted with MA105.

Viral infection assays. We inoculated cells (4×10^4 cells per 200 μl in a 48-well plate) with viruses at 10 $CCID_{50}$ per cell for 1 h, washed them and incubated them in medium at 34 °C (for L-PSGL-1.1, Jurkat, U937, MOLT-4 or MT-2 cells) or 37 °C (for RD, HEp-2c, SK-N-MC or Vero cells). For mAb inhibition, we pretreated the cells with 10 μg ml^{-1} mAb for 1 h, washed them and maintained them in the medium with 10 μg ml^{-1} mAb. For inhibition with PSGL-1–Fc, we pretreated EV71-1095 (1×10^5 $CCID_{50}$) with 1 μg PSGL-1–Fc per 100 μl for 1 h and then inoculated them into L-PSGL-1.1 cells. We incubated the cells for 1 h in the presence of PSGL-1–Fc, washed them and maintained them in the absence of PSGL-1–Fc. We subjected the culture supernatants and infected cells to three cycles of freeze-thawing before titration.

Statistical analyses. We carried out all infection assays in triplicate and compared the mean viral titers with Student's *t* test (two-tailed). We considered *P* values of <0.01 statistically significant.

29. Kitamura, T. & Morikawa, Y. Isolation of T-cell antigens by retrovirus-mediated expression cloning. *Methods Mol. Biol.* **134**, 143–152 (2000).

JOURNAL OF VIROLOGY, Mar. 2009, p. 2510–2517 Vol. 83, No. 6
0022-538X/09/$08.00+0 doi:10.1128/JVI.02416-08

Mitogen-Activated Protein Kinase-Activated Kinase RSK2 Plays a Role in Innate Immune Responses to Influenza Virus Infection▽

Satoshi Kakugawa,[1] Masayuki Shimojima,[1] Hideo Goto,[1] Taisuke Horimoto,[1] Naoki Oshimori,[3] Gabriele Neumann,[5] Tadashi Yamamoto,[3] and Yoshihiro Kawaoka[1,2,4,5]*

Division of Virology, Department of Microbiology and Immunology, Institute of Medical Science, University of Tokyo, 4-6-1 Shirokanedai, Minato-ku, Tokyo 108-8639, Japan[1]; Exploratory Research for Advanced Technology (ERATO), Japan Science and Technology Agency, Saitama 332-0012, Japan[2]; Division of Oncology, Institute of Medical Science, University of Tokyo, 4-6-1 Shirokanedai, Minato-ku, Tokyo 108-8639, Japan[3]; International Research Center for Infectious Diseases, Institute of Medical Science, University of Tokyo, Tokyo 108-8639, Japan[4]; and Department of Pathobiological Sciences, School of Veterinary Medicine, University of Wisconsin, Madison, Wisconsin 53706[5]

Received 24 November 2008/Accepted 29 December 2008

Viral infections induce signaling pathways in mammalian cells that stimulate innate immune responses and affect cellular processes, such as apoptosis, mitosis, and differentiation. Here, we report that the ribosomal protein S6 kinase alpha 3 (RSK2), which is activated through the "classical" mitogen-activated protein kinase pathway, plays a role in innate immune responses to influenza virus infection. RSK2 functions in the regulation of cell growth and differentiation but was not known to play a role in the cellular antiviral response. We have found that knockdown of RSK2 enhanced viral polymerase activity and growth of influenza viruses. Influenza virus infection stimulates NK-κB- and beta interferon-dependent promoters. This stimulation was reduced in RSK2 knockdown cells, suggesting that RSK2 executes its effect through innate immune response pathways. Furthermore, RSK2 knockdown suppressed influenza virus-induced phosphorylation of the double-stranded RNA-activated protein kinase PKR, a known antiviral protein. These findings establish a role for RSK2 in the cellular antiviral response.

Influenza A viruses cause highly contagious respiratory infections in humans and several animal species (reviewed in reference 51). Annual epidemics account for an estimated 20,000 excess deaths and 100,000 excess hospitalizations in the United States alone. Pandemics occur at irregular intervals and can claim millions of lives, as witnessed with the "Spanish influenza" in 1918 and 1919, which killed an estimated 40 to 50 million people worldwide.

Influenza A viruses belong to the family *Orthomyxoviridae* and possess eight segments of single-stranded, negative-sense RNA, which encode 10 or 11 proteins (reviewed in reference 36). Four viral proteins—the polymerase subunits PB2, PB1, and PA and the nucleoprotein NP—are required for the replication and transcription of the viral RNA (vRNA). Two viral surface glycoproteins (hemagglutinin and neuraminidase [NA]) are critical for virus binding and release and are the major viral antigens. The NS1 protein is a multifunctional factor that counteracts the cellular interferon (IFN) responses that are triggered upon influenza virus infection (4, 9, 12, 21, 29, 30, 48, 49). Other viral proteins play a critical role(s) in the nuclear export of newly synthesized viral replication complexes (i.e., the matrix protein M1 and the nuclear export protein NS2), virus entry (i.e., the ion channel protein M2), and the regulation of apoptosis (i.e., the PB1-F2 protein, which is not encoded by all influenza A virus strains); the functions of these proteins are described in detail in reference 36.

Stimuli such as stress, cytokines, mitogens, and viral infections trigger multiple signaling cascades, such as the mitogen-activated protein kinase (MAPK) pathways, in mammalian cells (reviewed in references 10, 40, and 41). MAPK signaling pathways regulate critical cellular activities, such as gene expression, metabolism, apoptosis, mitosis, and differentiation. In the "classical" MAPK pathway, Raf-1 (a serine/threonine kinase) activates MEK1/2 (a MAPK kinase kinase), which subsequently activates the MAPK kinase extracellular signal-regulated kinases 1 and 2 (ERK1/2). In addition to ERK1/2, several other MAPK family members have been identified in mammalian cells, including p38 isoforms, c-Jun amino-terminal kinases, and BMK/ERK5 (big MAPK). MAPKs can activate their targets through direct phosphorylation or through the phosphorylation of downstream kinases (MAPK-activated protein kinases). Prominent examples of MAPK-activated protein kinases are p90 ribosomal S6 kinases (RSKs), which have emerged as major downstream mediators of ERK signal transduction (reviewed in references 6 and 41). In mammals, four RSKs (RSK1 to -4) have been identified; these are ubiquitously expressed and promote cell growth, proliferation, and cell survival (the last by interfering with apoptotic effectors). Despite their role as downstream mediators of ERK signal transduction, RSKs were not previously known to have antiviral effects.

Influenza virus infection has been shown to activate all known MAPK pathways (reviewed in references 26 and 27). Influenza virus-induced activation of the p38 and c-Jun amino-terminal kinase pathways seems to trigger antiviral effects (23,

* Corresponding author. Mailing address: Division of Virology, Department of Microbiology and Immunology, Institute of Medical Science, University of Tokyo, 4-6-1 Shirokanedai, Minato-ku, Tokyo 108-8639, Japan. Phone: 81-3-5449-5310. Fax: 81-3-5449-5408. E-mail: kawaoka@ims.u-tokyo.ac.jp.

▽ Published ahead of print on 7 January 2009.

25), while activation of the ERK1/2 and big MAPK pathways likely supports influenza virus replication (39). Further studies are needed to establish the significance of these signaling pathways for influenza virus replication.

Influenza virus infection also activates the IκB kinase/NF-κB pathway (reviewed in reference 19). This pathway is activated by a number of other viruses and leads to the expression of proinflammatory and antiviral cytokines, including beta IFN (IFN-β) and tumor necrosis factor alpha. The role of NF-κB activation in the context of influenza virus infection is still unclear, as two studies found a virus-supportive role (32, 50) and another study suggested that NF-κB activation is not required for efficient influenza virus replication (5).

In this study, we provide evidence that the MAPK-activated protein kinase ribosomal protein S6 kinase alpha 3 (RSK2) is activated upon influenza virus infection and that this kinase affects antiviral responses through NF-κB, IFN-β, and a known antiviral factor, PKR. These findings establish a novel antiviral role for RSK2.

MATERIALS AND METHODS

Cell culture. Human embryonic kidney cells (293T cells and 293 cells) were cultured in Dulbecco's modified Eagle's medium (DMEM; Sigma) supplemented with 10% heat-inactivated fetal calf serum (FCS) and antibiotics. Plat-GP (murine leukemia virus-based packaging) cells were kindly provided by T. Kitamura (University of Tokyo, Tokyo, Japan) and cultured in DMEM with 10% FCS and 10 μg/ml blasticidin (Invitrogen). QT6 quail fibrosarcoma cells were maintained in Ham's F-12K medium (MP Biomedicals) supplemented with 10% FCS and 10% tryptose phosphate broth (Sigma). Madin-Darby canine kidney (MDCK) cells were cultured in minimal essential medium containing 5% newborn calf serum and antibiotics.

Viruses. PB2-627K- and PB2-627E-expressing influenza viruses were generated by reverse genetics (31) and propagated in MDCK cells. Both viruses possess the hemagglutinin and NA genes of A/WSN/33 (H1N1) virus, while the remaining genes were derived from A/Hong Kong/483/97 (H5N1) virus; the PB2 protein of this virus possesses a lysine at position 627, resulting in PB2K virus. PB2E virus is a derivative that possesses glutamic acid at position 627 in the PB2 protein. Influenza virus B/Hong Kong/73 and Sendai virus (Enders strain; kindly provided by Allan Portner, St. Jude Children's Research Hospital, Memphis, TN) were also propagated in MDCK cells. Viruses were titrated by plaque assay in MDCK cells.

Plasmids. The PB1, PA, and NP proteins of A/Hong Kong/483/97 (H5N1) virus were expressed with the pMX vector (34), which was kindly provided by T. Kitamura, University of Tokyo, Tokyo, Japan. For the PB2 protein, we used a variant that possesses glutamic acid at position 627 (PB2E). pPolI-fCD2 and pPolI-Luc drive the synthesis of negative-sense vRNAs comprising the 3′ noncoding region of the NA (A/Hong Kong/483/97) vRNA, the complementary coding sequence of luciferase or feline CD2 (fCD2) (45), respectively, and the 5′ noncoding region of the NA vRNA.

Gallus gallus RSK2 and human PKR were cloned from chicken embryo fibroblasts or human 293T cells, as appropriate. Briefly, RNA was extracted from these cells by use of the RNeasy minikit (Qiagen). Reverse transcription-PCR was performed with an oligo(dT) primer followed by PCR with gene-specific primers. The PCR products were cloned into the pCAGGS vector (under the control of the chicken β-actin promoter [33]) and then sequenced. To escape the knockdown effect of the short hairpin RNA (shRNA), a silent mutation was introduced into the human RSK2 protein expression plasmid, yielding pmRSK2.

pNF-κB-Luc, which expresses luciferase upon promoter activation by NF-κB, was purchased from Stratagene. pIFN-luc, which express luciferase under the control of an IFN-β-dependent promoter, was derived from the following components: the bacterial artificial chromosome clone RP11-113D19, which was used as the source of the promoter and terminator regions of the human IFN-β gene (Invitrogen), and pGEM-luc (Promega), which was used as the source of the luciferase gene. These components were joined by PCR, and the resulting construct was cloned into the pUC19 vector.

cDNA library. A cDNA library was prepared from quail QT6 cells by isolating mRNA (with the FastTrack 2.0 mRNA isolation kit; Invitrogen). cDNA was synthesized by use of the SuperScript Choice system for cDNA synthesis (Invitrogen), according to the manufacturer's instructions. The resulting cDNAs were size fractionated by agarose gel electrophoresis, and cDNA fragments longer than 1 kbp were extracted from the gel with the Qiaex II gel extraction kit (Qiagen). The respective cDNA fragments were then inserted into the BstXI sites of pCAGGS-Kan (a pCAGGS variant that carries the kanamycin resistance gene) by using BstXI adapters (Invitrogen). The ligated DNA was ethanol precipitated and then electroporated into DH10B competent cells.

Library screening. Human embryonic kidney 293T cells were transfected with plasmids for the expression of the polymerase and NP proteins, i.e., pMX-PB2E (possessing glutamic acid at position 627), -PB1, -PA, -NP; with the plasmid for the synthesis of a virus-like RNA encoding fCD2 (polI-fCD2); and with the quail QT6 cDNA library. Cells were incubated for 2 days at 33°C, collected, and treated with an antibody against fCD2 (44, 45). After incubation at 4°C for 30 min, fCD2-positive cells were selected by immunoaffinity with Bio-Adembeads goat anti-mouse immunoglobulin M (IgM) antibody (Ademtech) according to the manufacturer's instructions. Plasmid DNA was then extracted from the cells and amplified in *Escherichia coli* in Luria-Bertani medium supplemented with kanamycin. Selection of cells that expressed high levels of fCD2 was repeated four times, at which point plasmid DNA was extracted from the cells and sequenced.

Luciferase assay. Luciferase assays were performed by use of a dual-luciferase reporter assay system (Promega) on a microplate luminometer (Veritas; Turner Biosystems, Sunnyvale, CA), according to the manufacturer's instructions. As an internal control for the dual-luciferase assay, pGL4.74[hRluc/TK] (Promega) was used.

Construction of RSK2 knockdown cells by use of a retroviral vector. shRNA with a human RSK2 target sequence (5′-GATGCTGCTTGTGATATATGG-3′) was flanked by the mU6 promoter and terminator. The resulting cDNA was inserted into the pSSSP vector, which was kindly provided by H. Iba (University of Tokyo, Tokyo, Japan). A similar plasmid, pSSSP-shGFP, with a target sequence for green fluorescent protein (GFP) (5′-GCCACAACGTCTATATCA TGG-3′) was also kindly provided by H. Iba (University of Tokyo, Tokyo, Japan). These plasmids were used to produce murine leukemia virus-based viruses in Plat-GP cells, as described previously (20, 45), and then used to transduce 293 cells.

Analysis of virus propagation. To establish virus growth rates, three wells of cells were infected in parallel with virus at a multiplicity of infection (MOI) of 0.05 and incubated at 33°C or 37°C. At various times, supernatants were assayed to determine the titer of the infectious virus by plaque assay of MDCK cells.

NF-κB and IFN-β promoter activity. pNF-κB-Luc and pIFN-luc were transfected into 293 (human embryonic kidney) cells with a retroviral vector expressing shRNA specific to human RSK2 (shRSK2 cells) and shGFP cells, respectively. Nine hours later, cells were infected with virus at an MOI of 1.0 and incubated at 33°C. Twelve hours later, the levels of luciferase expression were determined.

Western blot analysis. To assess RSK2 expression levels, shRSK2 cells and shGFP cells were suspended in Tris-glycine sodium dodecyl sulfate (SDS) sample buffer (Invitrogen), and Western blot analysis was performed with anti-RSK2 (E1; Santa Cruz Biotechnology) and anti-β-actin (as an internal control; Sigma) antibodies, according to the manufacturers' instructions. Biotinylated anti-mouse IgG antibody (Vector) was used as a secondary antibody. Bands were detected with the Vectastain ABC kit (Vector) and ECL Plus Western blotting detection reagents (GE Healthcare); the VersaDoc imaging system (Bio-Rad) was used to quantify band intensities.

To analyze expression of the viral M1 protein, shRSK2 cells and control shGFP cells were infected with a PB2-627E-expressing virus at an MOI of 1.0 and incubated at 33°C. At various times, the cells were washed three times with phosphate-buffered saline and resuspended in Tris-glycine SDS sample buffer. Western blot analysis was performed with monoclonal antibodies specific to the M1 protein, with β-actin as a control. Biotinylated anti-mouse IgG antibody (Vector) was used as a secondary antibody. Bands were detected as described above.

To assess RSK2 phosphorylation levels, 293 cells (7.5×10^5 cells) were plated in 60-mm plates and cultured overnight at 37°C. The growth medium was replaced with DMEM containing 4% bovine serum albumin, and cells were infected with influenza virus (MOI of 3.0) 12 hours later; control cells remained uninfected. Three hours postinfection, RSK2 was immunoprecipitated with anti-RSK2 antibody (E1; Santa Cruz) coupled to protein G beads. The beads were resuspended in Tris-glycine SDS sample buffer, and Western blot analysis was performed with antibodies specific for RSK phosphorylated at Thr365/Ser369, Ser386, or Thr577 (antibodies obtained from Cell Signaling). Biotinylated anti-rabbit IgG antibody (Vector) was used as a secondary antibody. Bands were detected as described above.

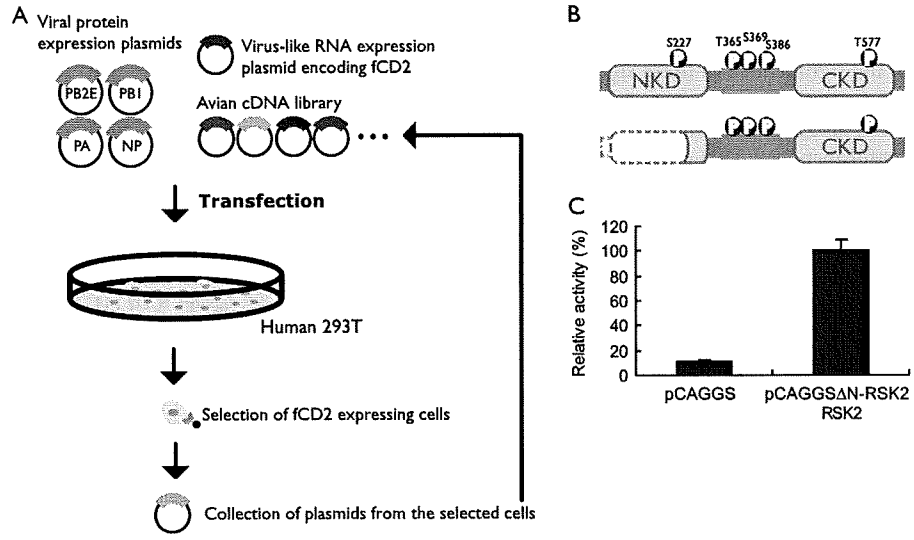

FIG. 1. Identification of cellular proteins that enhance influenza virus replication and downregulation of influenza virus replication by RSK2. (A) Human embryonic kidney 293T cells were transfected with plasmids encoding the components of the influenza viral replication complex (PB2, PB1, PA, and NP). The PB2 protein possesses glutamic acid at position 627 (PB2-627E), which supports efficient replication in avian cells but not in mammalian cells at 33°C. Cells were cotransfected with a plasmid for the synthesis of a virus-like RNA encoding fCD2 (polI-fCD2) and with an avian (quail cell) cDNA library. Cells expressing avian proteins that support efficient replication by PB2-627E virus in mammalian cells at 33°C will produce increased amounts of fCD2. Cells with high levels of fCD2 were selected by immunoaffinity using anti-fCD2 antibody. After a total of four rounds of selection, plasmid DNA was extracted from the cells and sequenced. (B) Schematic diagram of human RSK2 (top) and the N-terminally deleted avian RSK2 protein selected in our screening approach (bottom). The CKD is activated by ERK1/2, resulting in the activation of the NKD. The NKD subsequently phosphorylates target proteins. (C) Influenza viral polymerase activity in 293T cells expressing avian ΔN-RSK2. Cells were transfected with plasmids expressing PB2E, PB1, PA, and NP; a virus-like RNA encoding luciferase (pPolI-luc); and the N-terminally deleted avian RSK2 protein (pCAGGS-ΔN-RSK2) or the "empty" control vector (pCAGGS). Cells were maintained at 33°C for 24 h and were then subjected to luciferase assays. In human cells at 33°C, expression of N-terminally deleted avian RSK2 increased the activity of a replication complex possessing glutamic acid at position 627 in the PB2 protein. The error bars represent standard deviations from three independent experiments.

To assess the phosphorylation levels of PKR, shRSK2 and control shGFP cells were infected at an MOI of 0.01 or 1.0 with influenza virus and incubated at 33°C. Infected cells were collected at 0, 6, and 12 h postinfection. Western blot analysis was performed with anti-PKR (Santa Cruz), anti-phospho-PKR (Biosource), and anti-β-actin (as an internal control; Sigma) antibodies according to the manufacturers' instructions. Biotinylated anti-rabbit IgG antibody or anti-mouse IgG antibody was used as a secondary antibody. Bands were detected as described above.

Statistical analysis. Student's *t* test was used to determine statistical significance.

RESULTS AND DISCUSSION

Relatively little is known about the host factors that interact with influenza virus components. The influenza virus PB2 protein is now recognized as a critical determinant of pathogenicity and host range restriction (16, 17, 28, 46, 47). In general, lysine 627 of the PB2 protein confers a high level of pathogenicity to influenza viruses in mammals (16), which can be modeled by efficient replication in mammalian cells at 33°C and 37°C (17). In contrast, viruses with a glutamic acid residue at this position (PB2-627E) have low pathogenicity in mammals (16) and attenuated virus replication in mammalian systems at 33°C and, to a lesser extent, at 37°C (17). In order to identify the host factor(s) that restricts PB2-627E virus growth in mammalian cells, we transfected human embryonic kidney (293T) cells with a plasmid for synthesis of an influenza virus-like RNA. This virus-like RNA encodes fCD2; fCD2 thus serves as a reporter protein (45) to assess viral replication efficiencies. We cotransfected cells with plasmids for expression of the A/Hong Kong/483/97 (H5N1) virus NP, PB1, and PA proteins and a plasmid for expression of a mutant PB2, PB2-627E (Fig. 1A). The PB2-627E mutation restricts amplification of the virus-like RNA in human cells at 33°C. To identify the avian host factor(s) that "rescues" efficient replication, even with PB2-627E, we cotransfected human 293T cells with a cDNA expression library derived from avian quail QT6 cells. Avian host factors that mediate efficient replication of PB2-627E virus should support high levels of fCD2 expression from the virus-like RNA. The fCD2-positive cells were selected with an antibody against fCD2. After four rounds of selection, we extracted plasmids from the fCD2-positive transfectants and subjected them to sequencing.

One of the identified host proteins was the quail homolog of the *Gallus gallus* RSK2, from which 310 N-terminal amino acids were missing (avian ΔN-RSK2) (Fig. 1B). To confirm that avian ΔN-RSK2 enhances influenza virus replication in mammalian cells at 33°C, we overexpressed this protein in human cells that expressed the viral replication complex components (i.e., PB2-627E, PB1, PA, and NP) and a virus-like RNA that encodes the luciferase reporter protein. Our results indicate that luciferase expression was elevated in cells expressing avian ΔN-RSK2 protein relative to that in control cells expressing the "empty" expression vector (Fig. 1C).

Next, we cloned the full-length avian and human RSK2 proteins and tested their ability to enhance PB2-627E-mediated replication in human cells at 33°C; however, we did not detect a significant effect for either protein (data not shown).

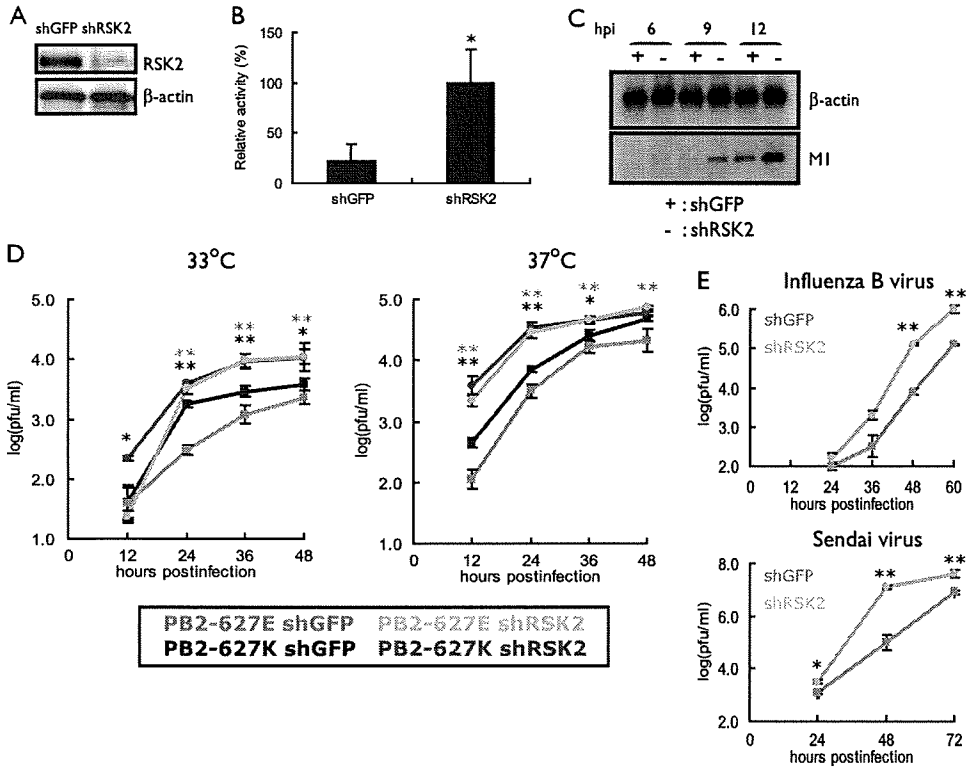

FIG. 2. Effect of RSK2 knockdown on influenza virus replication. (A) Knockdown of human RSK2. 293 cells were transduced with retroviral vectors for shRNAs to human RSK2 or GFP (as a control), resulting in shRSK2 and shGFP cells. RSK2 expression levels were assessed by Western blotting with an antibody to this protein. β-Actin expression levels served as an internal control. (B) Viral polymerase activity in shRSK2 and shGFP cells. Cells were transfected with plasmids that directed synthesis of PB2-627E, PB1, PA, NP, and pPolI-luc. After incubation at 33°C for 24 h, cell lysates were prepared and subjected to luciferase assays. Knockdown of RSK2 resulted in more-efficient replication of the virus-like RNA, suggesting that RSK2 suppresses influenza virus replication. The error bars represent standard deviations from three independent experiments. The statistical significance of the difference between the control and test samples is shown by the *P* value, which was determined by Student's *t* test (*, $P < 0.05$). (C) Viral protein production in shRSK2 cells and shGFP cells. shRSK2 and shGFP cells were infected with virus possessing PB2-627E and incubated at 33°C. At the indicated time points postinfection, Western blot analysis was carried out with antibodies against M1 and β-actin. (D) Influenza A virus growth in shRSK2 cells. shRSK2 and control shGFP cells were infected at an MOI of 0.05 with PB2-627E or PB2-627K virus, which possesses glutamic acid or lysine at position 627 in the PB2 protein, respectively. Cells were incubated at 33°C or 37°C for the indicated time periods. Virus titers in MDCK cells were determined. The error bars represent standard deviations from three independent experiments. The statistical significance of the difference between the control and test samples is shown by *P* values, which were determined by Student's *t* test (**, $P < 0.01$; *, $P < 0.05$; black asterisks indicate the PB2-627K virus, and gray asterisks indicate the PB2-627E virus). (E) Influenza B virus and Sendai virus growth in shRSK2 cells. shRSK2 and control shGFP cells were infected at an MOI of 0.05 with influenza B virus or Sendai virus. At the indicated times after infection, cells were harvested and the virus titers in MDCK cells were determined. The error bars represent standard deviations from three independent experiments. The statistical significance of the difference between the control and test samples is shown by the *P* value, which was determined by Student's *t* test (**, $P < 0.01$; *, $P < 0.05$).

RSK family members are unusual among serine/threonine kinases in that they contain two distinct kinase domains that are sequentially activated (Fig. 1B). The C-terminal kinase domain (CKD) is activated by ERK1/2, which then triggers subsequent activation of the N-terminal kinase domain (NKD) (reviewed in reference 6). The NKD of RSK2 then phosphorylates a broad range of substrates, including cAMP response element-binding protein, c-Fos, glycogen synthase kinase 3, and many others (reviewed in reference 6). ΔN-RSK2 contains the entire CKD of this protein (Fig. 1B) and may sequester free ERK1/2, thereby preventing activation of functional RSK2. Thus, we speculated that full-length RSK2 has antiviral activity and that ΔN-RSK2 acts as a dominant-negative factor that suppresses RSK2 and its antiviral activity, resulting in increased viral replication.

To test our hypothesis that RSK2 has antiviral activity against influenza virus, we knocked down RSK2 in 293 (human embryonic kidney) cells using a retroviral vector expressing shRNA specific to human RSK2. RSK2 expression was reduced to approximately 15% in shRSK2 cells relative to the expression level in control shGFP cells, which express shRNA against GFP (Fig. 2A). As speculated, RSK2 knockdown resulted in increased viral polymerase activity for PB2-627E at 33°C (Fig. 2B) and, as a consequence, resulted in increased production of the viral M1 protein (Fig. 2C).

The data obtained thus far indicate that RSK2 suppresses influenza virus replication. However, the question of whether RSK2 interferes with influenza virus replication in general or in a strain- or host-specific manner remains unanswered. To address this question, we generated influenza viruses that possessed either a lysine at position 627 of PB2 (PB2-627K), which confers efficient replication in mammalian cells at 33°C and

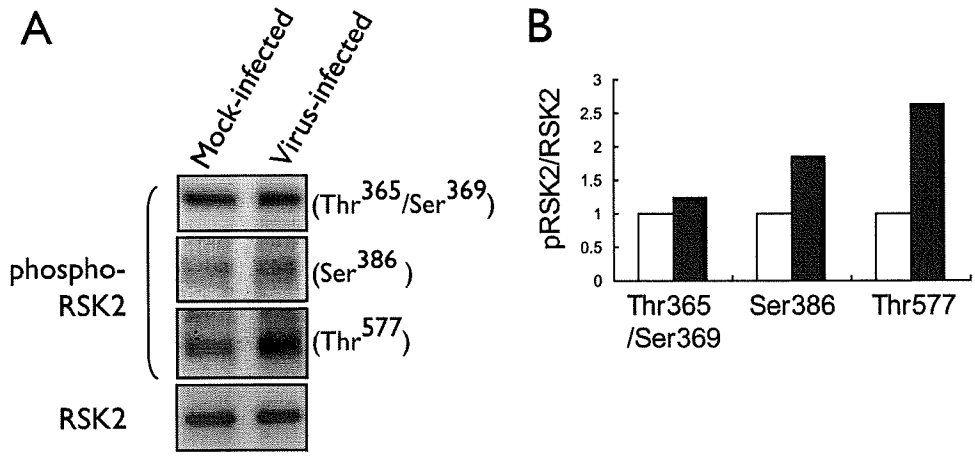

FIG. 3. Influenza virus-induced phosphorylation of RSK2. (A) 293 cells were infected with the PB2-627K virus (MOI of 3.0) or remained mock infected. Three or 5 hours later, cell lysates were immunoprecipitated with anti-RSK2 antibody, followed by Western blot analysis with the indicated antibodies to phosphorylated forms of RSK2. (B) Graphical representation of data shown in panel A. The relative ratios of phosphorylated to nonphosphorylated RSK2 are depicted. Influenza virus infection results in phosphorylation of RSK2. White bars, mock-infected cells; black bars, virus-infected cells.

37°C, or a glutamic acid at this position (PB2-627E), which results in attenuation of replication in mammalian cells at 33°C and, to a lesser extent, at 37°C. Growth of both viruses at 33°C and 37°C in shRSK2 cells and control shGFP cells was tested. Briefly, cells were infected at an MOI of 0.05 with PB2-627E or PB2-627K virus and virus titers in the culture supernatant were determined by plaque formation assays of MDCK cells at various times postinfection. As expected, the PB2-627K virus grew more efficiently than the PB2-627E virus in control shGFP cells at 33°C (Fig. 2D, left), while only minor differences in growth were observed for PB2-627K and PB2-627E viruses in control shGFP cells at 37°C (Fig. 2D, right); these findings are consistent with our earlier data (17). By comparing viral growth properties in control shGFP and shRSK2 cells, we found more-efficient growth in shRSK2 cells for both viruses at both temperatures, demonstrating that the nature of the amino acid at position 627 of PB2 does not affect the antiviral effect mediated by RSK2; all subsequent infection experiments were therefore carried out with the PB2-627K virus. Together, these findings indicate that RSK2 is a general antiviral host factor that suppresses influenza A virus replication.

To further examine the antiviral function of RSK2, we assessed the growth kinetics of an influenza B virus and Sendai virus (a negative-sense RNA virus belonging to the family *Paramyxoviridae*) in shRSK2 and shGFP control cells (Fig. 2E). These viruses grew more efficiently in shRSK2 cells than in control shGFP cells. Hence, RSK2 may have broad antiviral effects; for example, it may trigger an innate immune responses.

In quiescent cells, RSK2 is maintained in an inactive form in a complex with ERK1/2 (reviewed in reference 42). Interaction with phosphorylated ERK1/2 results in RSK2 phosphorylation, dissociation from ERK1/2, and (partial) translocation to the nucleus (7). To assess whether RSK2 is activated upon influenza virus infection, we immunoprecipitated RSK2 from cell lysates obtained from influenza virus- or mock-infected cells and subsequently evaluated the phosphorylation status of RSK2 using antibodies specific to distinct phosphorylated forms of RSK2. Influenza virus infection resulted in increased levels of phosphorylated RSK2 compared to those in mock-infected cells (Fig. 3A and B). The most efficient induction of phosphorylation was observed for Thr577. This residue is phosphorylated by ERK1/2, resulting in the activation of RSK2 and the subsequent autophosphorylation of other phosphorylation sites, such as Ser386 (reviewed in reference 6). The observed phosphorylation of RSK2 upon influenza infection may result from direct interaction with a viral component or from ERK1/2 signaling, as the "classical" MAPK (Raf/MEK/ERK) pathway is known to be activated by influenza virus infection (38).

Next, we assessed the mechanism(s) by which RSK2 affects influenza virus replication. RSK2 activates NF-κB (13, 43), a major player in innate immune responses to viral infections (reviewed in reference 19). Moreover, NF-κB is known to be activated upon influenza virus infection (35). Therefore, we speculated that influenza virus-induced activation of RSK2 may lead to the stimulation of NF-κB and subsequent induction of an antiviral response. To test this assumption, we expressed the luciferase reporter protein under the control of an NF-κB-dependent promoter in virus- or mock-infected shRSK2 and control shGFP cells (Fig. 2A). As expected, influenza A virus infection induced NF-κB promoter activity in shGFP cells (Fig. 4A); the level of promoter stimulation was similar to that published elsewhere (52). In contrast, no significant increase in NF-κB-dependent promoter activity was observed in virus-infected shRSK2 cells (Fig. 4A), suggesting that virus-induced NF-κB stimulation relies on RSK2 activation. This lack of activation was partially restored following transfection of shRSK2 cells with pmRSK2, which encodes a human RSK2 cDNA containing a silent mutation within the small interfering RNA target sequence (Fig. 4A). In conclusion, these findings suggest that RSK2 may affect influenza virus replication, at least in part, through NF-κB.

NF-κB stimulation leads to the expression of multiple cellular factors, including IFN-β, a central player in the innate immune response that is activated upon virus infection. We asked whether RSK2 activates IFN-β-stimulated promoters.

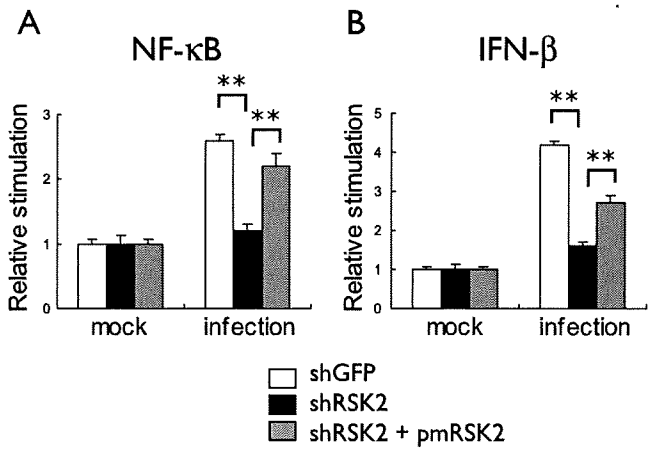

FIG. 4. Effect of RSK2 knockdown on influenza virus-induced activation of NF-κB- and IFN-β-dependent promoters. Plasmids that express luciferase under the control of NF-κB (A)- or IFN-β-dependent (B) promoters were transfected into shRSK2 or control shGFP cells. Nine hours posttransfection, cells were infected with the PB2-627K virus at an MOI of 1; control cells remained mock infected. After 12 hours of incubation at 33°C, cell lysates were prepared and subjected to luciferase assays. In a parallel experiment, cells were also transfected with pmRSK2, which encodes a silently mutagenized human RSK2 that is not recognized by the RSK2 shRNA. Influenza virus induced stimulation of NF-κB- and IFN-β-dependent promoters in shGFP cells (white bars); this stimulation is blocked by RSK2 knockdown (black bars) but can be partially restored upon expression of RSK2 that is insensitive to the RSK2 shRNA (gray bars). The error bars represent standard deviations from three independent experiments. *P* values were determined by Student's *t* test (**, $P < 0.01$).

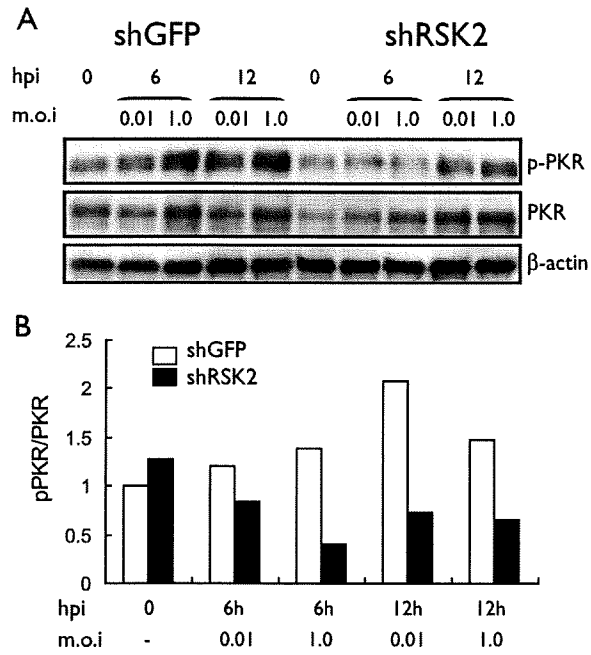

FIG. 5. Effect of RSK2 knockdown on influenza virus-induced phosphorylation of PKR. (A) shRSK2 cells and control shGFP cells were infected with the PB2-627K virus at an MOI of 0.01 or 1 and incubated at 33°C. At the indicated times postinfection, cell lysates were prepared and subjected to Western blot analysis with antibodies against PKR, phosphorylated PKR, or β-actin, which served as an internal control. hpi, hours postinfection. (B) Graphical representation of data shown in panel A. The relative ratios of phosphorylated to nonphosphorylated PKR are depicted. Influenza virus infection results in increased levels of phosphorylated PKR in control shGFP cells but not in shRSK2 cells.

We carried out experiments essentially as described in the previous section. That is, we cloned the luciferase gene under the control of an IFN-β-stimulated promoter and assayed luciferase expression in virus- and mock-infected shRSK2 and control shGFP cells (Fig. 4B). Influenza virus infection activated IFN-β-stimulated promoter activity in control shGFP cells (Fig. 4B) but not in shRSK2 cells (Fig. 4B). This impediment was partially overcome by transfection of shRSK2 cells with pmRSK2 (Fig. 4B). These results demonstrate that RSK2 activates both NF-κB and IFN-β signaling pathways upon influenza infection in 293 cells.

PKR is an important component of IFN-mediated antiviral responses (reviewed in reference 15). This kinase phosphorylates the α subunit of eukaryotic initiation factor 2, resulting in rapid inhibition of translation and restriction of the spread of the virus (2, 3, 11, 14). Recently, PKR was also identified as an RSK2 substrate (53). We tested whether RSK2 affects influenza virus replication through PKR phosphorylation and activation. As expected, phosphorylation of PKR upon influenza virus infection was apparent in control shGFP cells (Fig. 5A; Fig. 5B shows an increasing ratio of phosphorylated to nonphosphorylated PKR upon virus infection). In contrast, PKR phosphorylation was suppressed in shRSK2 cells (Fig. 5A and B), indicating that influenza virus-induced activation of RSK2 results in PKR phosphorylation in 293 cells.

In summary, we demonstrated that the MAPK-activated protein kinase RSK2 plays a role in the innate immune response to influenza virus infection, as shown in Fig. 6. RSK2 is known to phosphorylate cellular factors involved in cell proliferation, regulation of transcription, regulation of translation, cell survival, and apoptosis (reviewed in reference 6) and may affect viral growth through these processes. The human immunodeficiency virus Tat protein is known to interact with RSK2 (18), resulting in RSK2 activation. Activated RSK2 is, in turn,

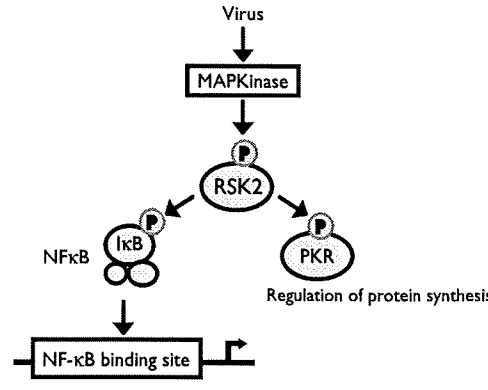

FIG. 6. Putative role of RSK2 in antiviral signaling. Influenza virus infection may activate RSK2 through MAPK kinase signaling pathways or through direct interaction with a viral component. Our data suggest that RSK2 activation is needed for efficient stimulation of NF-κB, IFN-β, and PKR, all of which play major roles in the cellular antiviral response.